C. P. No. 618

C. P. No. 618

MINISTRY OF AVIATION

AERONAUTICAL RESEARCH COUNCIL

CURRENT PAPERS

A Comparison of Two Methods for Predicting the Potential Flow around Arbitrary Airfoils in Cascade

By

D. Pollard and J. Wordsworth

LONDON: HER MAJESTY'S STATIONERY OFFICE

1963

Price 8s 6d net

C.P. No.618

June, 1962

A COMPARISON OF TWO METHODS FOR PREDICTING THE POTENTIAL FLOW AROUND ARBITRARY AIRFOILS IN CASCADE

by

D. POLLARD and J. WORDSWORTH

Replaces A.R.C.23,814.

ACKNOWLEDGEMENT

The authors wish to express their appreciation of the advice and help given by Professor J.H. Horlock, Professor of Mechanical Engineering, University of Liverpool, at all stages of the production of this paper and also of the assistance given by Dr. A. Young and the staff of the Sub-Department of Numerical Analysis in the University of Liverpool.

INDEX

APPENDICES

1.0 SUMMARY

A method of conformal transformation due to Howell (B1) and a method of distributed singularities due to Schlichting (C1), for predicting the performance of cascades of arbitrary airfoils, have been adapted for use on an electronic computer. Much greater accuracy than hitherto is thus possible, and this has enabled numerous refinements to be made. For an airfoil section defined at 30 points, the former method requires about 4 hours equally divided between automatic computing and graphical work, while the latter is completely analytical and needs about 3 hours machine time (both times being for a slow code of computer operation). The two approaches are critically sensitive to profile shape. Pressure distributions as determined by each method are in close agreement, but the agreement in turning angle is only fair.

2.0 INTRODUCTION

There exists disturbing differences in cascade data as determined by American and British experiments, and in comparisons between these data and the limited amount of theoretical treatments at present available. The former disparity may be due to differences in experimental technique, because of difficulties in obtaining truly two dimensional flow in practice, while the latter is undoubtedly due to lack of an adequate theory. This paper outlines a study of two theoretical methods suggested by Howell (B1) and Schlichting (C1).

Among the methods available for solving the direct problem of the potential flow of a fluid through a cascade of arbitrary airfoils, a transformation method by Garrick (B4) may be mentioned; but like so many others, the usefulness of his method is severely limited by simplifications which are initially inherent, and approximations which are subsequently unavoidable, if a working solution is to be obtained. Of other classical treatments, two have been selected for study in this paper. Howell's approach was favoured because mathematically it is relatively simple and sound - the only approximation is in transforming an irregular circle into an exact circle. The Schlichting treatment found favour because it suggested a completely analytical approach, and lent itself readily to the study of a cascade with suction (c.f. American experimental technique). Both methods have as a starting point the basic profile shape of the arbitrary airfoil under investigation, and the performance of the cascade as determined by the said methods is very much dependent on the accuracy to which the profile is defined. Therefore the reliability of both treatments depends on the number of airfoil points which can be accommodated by the analysis, and this in the past has been the limiting factor. This limitation has been studied in detail in each approach, and the use of an electronic computer has brought about several improvements. With such a device, calculating time is no longer of prime importance - the limitations are now mathematical. Many difficulties were solved, but others arose; chief of these was the effect of profile shape, at the leading and trailing edges, on the pressure distribution round the blade. Mathematically, this is related to the rapidity with which a Fourier Series converges. It is true to say, that, the two approaches on an electronic computer having been exhaustively developed, the success of a calculation hinges on this major difficulty more than anything else.

Modifications of the Howell and Schlichting analyses were developed from calculations on cascades of 10C4/30C50 and NACA 65 -($12A_{10}$)10 blade profiles, because these are two profiles which, while having been designed basically for similar purposes, give the disturbing difference in performance referred to earlier. The development work was performed on these two profiles in compressor cascades at a stagger of 36°; it was then extended in the case of the British section to turbine and compressor cascades of 15° stagger. Thus the modified analyses have been investigated over a limited range of stagger, camber and thickness. To prove the value of the methods in general, they should be employed in a systematic investigation of all the possible combinations of stagger, camber and thickness likely to be met with in practice. Only then will the recommendations of this paper find universal application.

3.0 SYNOPSIS OF METHODS

3.1 The Method of Conformal Transformation

A series of conformal transformations, suggested by Howell (B1) and employed by Carter and Hughes (B2) reduces the flow through a cascade of known airfoils to that around a circular cylinder with circulation. The velocity at any point on the latter is easily calculated, whence the velocity at that point in cascade is found after multiplying by the velocity coefficient for each transformation performed.

The first transformation collapses the cascade into an isolated S - shaped contour; it is

$$\zeta = \tanh z.$$

A succession of Joukowski transformations

$$\zeta + \frac{C^2}{\zeta} = z$$

are used to transform the S-shaped contour into an irregular circle. The "optimum" irregular circle is sought - that is, one having the least number of irregularities. It is obtained after the minimum number (usually 2, 3 or 4) of Joukowski transformations, by careful choice of the axes and the parameter C. The optimum irregular circle is easily recognised, since the effect of a subsequent Joukowski transformation is to render the irregularities worse.

If the optimum irregular circle has no pronounced local irregularities, it can be transformed into an exact circle using the Theodorsen transformation

$$\sum_{1}^{n} \left[(A_r + i\ B_r)\ \zeta^{-r} \right] = \ln\ [z/\zeta]$$

in which the Fourier coefficients converge rapidly. Using 50 or 60 points to define the irregular circle, some 12 or so coefficients are sufficient to specify the Fourier Series. Should coefficients of higher order than the twelfth be not entirely negligible a better irregular circle should be sought.

The calculation is best performed for every point at which the airfoil is defined, and the choice of axes and parameter C (referred to above) is best obtained by hand. Experience has shown that although this may take about 30 minutes for each transformation, it is still less than an electronic computer requires using curve fitting programs, etc.

The method has been specially adapted for use on a Deuce Electronic Computer. Using a slow code of operation, the machine time required for a complete calculation, involving fixed cascade geometry and variable incidence, is approximately 2 hours. About 2 hours additional graphical work is necessary.

A full development of the method of conformal transformation is given in Appendix B.

3.2 The Method of Distributed Singularities

3.2.1. Basic Theory

The concept of singularities, and their use in the theoretical prediction of ideal fluid flow past solid bodies has been in use for many years and has been dealt with at length by various authors (eg. reference C10). Schlichting (reference C1) has used the method of singularities to determine the performance of two dimensional cascades of blades, in turbine and compressor configurations.

Sources, sinks and vorticies are distributed along a line corresponding to the position of the camber line of each blade in the cascade. The velocity induced by the sum of these singularities is calculated at points throughout the flow regime and added to the free stream velocity. The magnitude of the singularities is choosen so that a fluid streamline corresponds to each blade profile.

3.2.2. Approximations used in the analysis

To simplify analysis and bring calculation time down to a reasonable value the following three assumptions are made:-

(i) that a finite number of singularities are used to match the profile at a finite number of points. As the calculation requires the solution of a matrix of simultaneous equations, previous workers (references (C1) and (C2)) have limited themselves to three matching points. The authors of this paper have had the use of a "Deuce" digital computer and have extended the number of matching points to between 15 and 20.

(ii) that the blade profile can be split into a camber line and thickness distribution, which are considered separately (see figure C1) and (iii)that the singularities are distributed along the chord line, whence the induced velocities are calculated on the chord line, and corrected to give the velocity on the profile.

3.2.3. Basic equations

If at a given chordwise position $\frac{x}{c}$ the profile upper and lower ordinates are y_u and y_ℓ, the camber line ordinate and half thickness can be written, approximately,

$$y_s = \tfrac{1}{2}(y_u + y_\ell)$$

$$\text{and} \quad y_t = \tfrac{1}{2}(y_u - y_\ell)$$

With a source distribution $q(x)$ and vortex distribution $\gamma(x)$ the induced velocities at a point x, parallel to and perpendicular to the chord u, and v are such that, applying the continuity equation (see figure C1)

$$\frac{dy_t}{dx} = \frac{q(x)}{2(U + u)} \tag{3.2.1.}$$

and the slope of the camber line is given by,

$$\frac{dy_s}{dx} = \frac{V + v}{U + u} \tag{3.2.2.}$$

U, V are the components of the free stream, parallel and perpendicular to the chord.

Assuming $q(x)$, $\gamma(x)$ to be functions of a parameter ϕ where

$$\frac{x}{c} = \tfrac{1}{2}(1 - \cos\phi),$$

the distribution of singularities may be described in terms of a Fourier series and u and v calculated in terms of $q(x)$, $\gamma(x)$ for the cascade. The quantities $q(x)$, u and v are substituted in equations (3.2.1.) and (3.2.2.) with the Fourier coefficients as the unknown quantities. For every matching point on the profile (one value of y_t' and one value of y_s') a pair of simultaneous equations is produced and a pair of Fourier coefficients can be found. If n matching points are used, 2n simultaneous equations arise and the solution reveals 2n Fourier coefficients. The solution of 30 or more linear simultaneous equations is a task easily performed by the computer.

3.2.4. Computer time required for a calculation

The time required for a calculation on Liverpool University "Deuce" computer is 3¼ hours comprising:-

i) One and a half hours for calculating cascade parameter data, a function of stagger and space chord ratio.

ii) Half an hour to calculate thickness and camber line gradients

iii) One and a quarter hours to solve the simultaneous equations and calculate the pressure coefficients.

An extra half hour is required for each value of inlet angle α_1 after the first.

The programmes are written in "alphacode" which is comparatively slow, and could be rewritten in "basic" code, to produce quicker results now that the method has been shown to work.

A full development of the method and analysis is shown in appendices C and E.

4.0 CALCULATIONS ON CASCADES OF C4 AND NACA BLADES

Full details of the computational methods used are given in the appendices. The results of the various calculations made are now discussed.

4.1 The Method of Conformal Transformation Applied to a Cascade of 10C4/30C50 Airfoils, at a stagger of +36°, zero incidence

4.1.1. The pressure distribution (Fig.4.1.1.)

The pressure distribution shown is that derived from the flow around the irregular circle, with the leading edge point neglected. All the points lie on a smooth curve, with the exception of a few towards the trailing edge. The pressure distribution has not been constructed to pass through the theoretical stagnation point at the trailing edge, since this is not obtained in practice. The base profile is accurately defined in the region of the leading edge, and this has enabled a reliable determination of the suction and pressure peaks to be made.

4.1.2. The original and modified nose shapes (Fig.4.1.2.)

The leading edge point is neglected on the irregular circle, and the recalculated, effective nose shape is shown in Fig.(4.1.2.). The discrepancy as a result of neglecting the leading edge point is thus seen to be small. The pressure distribution of Fig.(4.1.1.) has slightly reduced suction and pressure peaks compared with the true C4 profile, since the modified nose shape is more slender.

4.1.3. The modified Fourier coefficients, Ar^1, Br^1

Graphical representation of the coefficients accentuates the asymptoting of the series to zero. In this example, it is seen that about 10 coefficients are sufficient to specify the series completely. This shows that the optimum irregular circle chosen has few irregularities, and these are small.

4.2. Method of Singularities Applied to Cascade of C4 Profile at 36° Stagger

Results of a specimen calculation are shown in graphs 4.2.1. to 4.2.5. The cascade is a compressor of 36° stagger and space-chord ratio unity. The pressure distribution has been determined for an inlet angle of 52.8° to compare with experimental data at present being obtained. The curve produced is smooth and the integrated lift coefficient compares favourably with that calculated from the turning angle, as shown in the table below. The blade profiles used are 10C4/30C50 profiles with a circular arc camber line, and a smooth pressure curve is produced from the measured gradients. In the case of a more irregular shape (eg. NACA 65(12A10)10) it is necessary to reduce the leading and trailing edge gradients. The effect of using this procedure on the C4 profile is shown in Fig.4.2.2.

There is little difference between this curve and the one for the original gradients shown in Fig.4.2.1.

The source and vortex distributions are shown in Fig.4.2.3. for the normal 10C4/30C50 profile and the recalculated camber line and thickness distribution shown in Figs.4.2.4. and 4.2.5. The recalculated camber line agrees well with that originally specified, but the thickness distribution shows some small discrepancy. The maximum difference between calculated and original thickness ordinates is ½% of the chord at 30% of the chord back from the leading edge.

TABLE I

Comparison of integrated and calculated parameters

	Integrated	Calculated	Percent Difference
Cp	0.720	0.728	1.1
$\frac{1}{c}\int\left(\frac{q(x)}{V_{m_x}}\right)d\left(\frac{x}{c}\right)$	0.005	0.000	
$\frac{1}{c}\int\left(\frac{\gamma(x)}{V_{m_x}}\right)d\left(\frac{x}{c}\right)$	0.517	0.531	2.6

4.3 Comparison of the two methods for calculations on a Cascade of 10C4/30C50 airfoils at zero incidence, various staggers

4.3.1., 4.3.2., 4.3.3. The Pressure distribution

(Figs.4.3.1., 4.3.2., 4.3.3.)

The agreement between the pressure distributions as determined by the two methods is close at the three staggers shown; therefore the calculation of the lift coefficients (which are proportional to the areas enclosed by the pressure curves) as determined by both methods is consistent. For positively staggered (compressor) cascades, the method of conformal transformation gives suction and pressure peaks which are slightly exaggerated compared to those determined by the method of singularities. At negative staggers, this is not so. The suction peak as determined by the Howell method occurs at about 10% chord; the method due to Schlichting yields a suction peak at about 15% chord.

4.3.4. Deviation as a function of stagger, and comparison with the rule for nominal deviation (Fig.4.3.4.)

In positively staggered cascades, the deviation determined by Howell's method is less, and that determined by Schlichting's method is greater, than that predicted by the rule for nominal deviation (B5). At low negative staggers, the Howell deviation increases above the nominal deviation, while the difference between the Schlichting deviation and nominal deviation increases as the stagger becomes very large, negative. These latter trends are, however, dependent on a calculation at one negative stagger in each case.

4.4. Further results using the method of singularities

Fig.4.4.1. shows the pressure distribution of a 10C4/10C50 profile blade in a 36^{o} stagger, 1.0 space-chord ratio configuration, for three different inlet angles. With a low (10^{o}) cambered profile a smooth curve is produced for all values of inlet angle, but at high angles of incidence the integrated lift coefficient shows a 5% error when compared with the calculated value.

Figs.4.4.2 and 4.4.3. show the pressure distribution for an NACA ($12A_{10}10$) profile in 36^{o} stagger 1.0 space-chord ratio compressor cascade. Fig.4.4.2. shows the original profile pressure distribution and Fig.4.4.3. the modified profile pressure distribution. The curves are of the same general shape but the number of calculated pressure coefficients which do not lie on the smooth curve has been reduced and the integrated lift coefficient compares more favourably with the calculated one in the second case than in the first.

5. CONCLUSIONS

5.1. Results of calculations using the method of conformal transformation and the method of singularities have been given in graphs 4.1 and 4.2 respectively. A comparison of the two methods at various staggers has been given in graphs 4.3.

5.2. The method of conformal transformation is mathematically exact and only two approximations are required in numerical computation. The Fourier series used (see paragraph B4) is limited to a finite number of terms and the irregular circle of the last transformation is smoothed at a point corresponding to the leading edge in order that this series may converge rapidly. The recalculated nose shape is very little different from the original and increases the length of the chord by only ½% (Fig.4.1.3.). A full explanation of these approximations is given in appendix B.

The pressure distribution obtained is a smooth curve and on integration the lift coefficient derived agrees with that produced by the turning angle, to within ½%. At the single space chord ratio investigated the method was found to be satisfactory over a wide range of stagger angles.

It is unlikely that this method will be transferred completely to a computer calculation, as the time required for curve fitting and the change of axes in the intermediate steps is rather long. The correct choice of the new axes between transformations requires a certain amount of experience if a reasonable transformation shape is to result. The change of axes by hand involves about half an hour's work.

5.3 The basic flow equations in the method of singularities contain the approximations mentioned in paragraph C.1. The results suggest that for the profile investigated these approximations are quite valid. Lift coefficients from the pressure distribution area and the turning angle agree within ½%, and the recalculated thickness distribution has a maximum discrepancy of ½% of the chord at the station of maximum thickness 30% (Fig.4.2.5.). Uninterrupted use may be made of a computer which allows a comparatively simple method of operation to be followed. Poor results are obtained from some profiles and the method is also unreliable at high angles of incidence (section 4.4). Large gradients in the camber line at the leading or trailing edges (e.g. as for the NACA 65($12A_{10}$)10 profile) cause irregularities in the calculated pressure distribution curves and thus the method would not be applicable to highly cambered turbine blades.

5.4. The outlet angle deviations from the two methods have been compared in Fig.4.3.4. Results from the method of conformal transformation predict a lower deviation for compressor cascades. The deviation derived from the method of singularities shows good agreement with the Howell-Carter nominal deviation rule. Pressure distributions from the two methods are in close agreement, with two small differences. The method of conformal transformation gives a slightly higher lift coefficient and a suction peak closer to the leading edge than the corresponding quantities from the method singularities (Fig.4.3).

5.5. Both methods have been adopted for use on a digital computer and certain approximations have been modified to allow full use to be made of computational accuracy.

The method of conformal transformation is more accurate analytically although the shape of the leading edge of the profile cannot be truely specified. The method is fairly slow as intermediate steps in the calculation have to be performed manually. For the cascades considered in this report the method has been found satisfactory over the range of stagger employed. The method of singularities, although containing mathematical approximations is straight forward and calculations are easily performed on a computer. No limit was found for stagger angle, but care must be taken that large values of profile gradients do not produce incorrect results. At large angles of incidence the method is inconsistant.

5.6. The method singularities is being developed to take account of boundary layer growth on the blade profile and the effect of a change in axial velocity across the cascade. It is hoped to present this analysis at a later date.

Appendix A NOTATION

The two methods of calculation set out in appendices B and C are so distinct that the notation for each is given under a separate heading. A1 contains the notation used in the method of conformal transformation, shown in appendix B and A2 the notation for the method of singularities in appendix C. An attempt has been made to use the same notation where possible, the most notable exception being the symbol for stagger angle, γ in appendix B and λ in appendix C.

A.1. The Method of Conformal Transformation

γ	stagger angle (positive for compressors, negative for turbines)
c	blade chord
s	blade spacing
p	static pressure at a point
V	velocity at a point
ρ	density of fluid
C_p	pressure coefficient at a point
p	an integer
q	an integer
r	an integer
n	an integer
i	imaginery quantity, equal to $\sqrt{-1}$
(X,Y)	cartesian co-ordinates in the basic airfoil
z	a complex plane
ζ	the transformed complex plane of z
(x,y)	cartesian co-ordinates in the plane of z
(ξ,η)	cartesian co-ordinates in the plane of ζ
(ξ',η')	the origin in a plane of ζ for the succeeding plane of z
K	the angle between the axis of ζ and the succeeding axis of x.
C	Joukowski parameter
A_r, B_r	Fourier coefficients

A_r^1, B_r^1	modified Fourier coefficients
λ	parameter in the plane of z
ϕ	argument in the plane of z
ψ	parameter in the plane of ζ
θ	argument in the plane of ζ
a	radius of base circle
r_0	radius of exact circle
Δ	increment in λ produced by Theodorsen transformation
ϵ	rotation of ϕ produced by Theodorsen transformation
α	flow angle relative to axial direction
(f,g,h), (m_1, m_2), (θ_1, θ_2)	parameters of the Theordorsen transformation

Subscripts:

0	a point on the airfoil
$-\infty$	a point at infinity upstream of the cascade
$+\infty$	a point at infinity downstream of the cascade
r	the rth term
a	axial direction
1	inlet conditions to the cascade
2	outlet conditions from the cascade
T.E.	the trailing edge point.

A.2. The Method of distributed Singularities

A_n, B_n	Fourier coefficients
C_p	Pressure coefficient
c	Blade chord length
K	Tan ϵ = V_{my}/V_{mx}
M	Combined, complex singularity strength (source and vortex)
n	An integer
P,Q,R,S	Simultaneous equation parameters
p_L	Local static pressure
p_1	Inlet pressure
q	Source strength

$q(x)$	Source strength distribution along x-axis
$R(F)$, $I(F)$, f,g	Intermediate calculation parameters
r, θ	Polar coordinates
s	Cascade blade pitch
$\frac{s}{c}$	Space chord ratio
U	A stream velocity
u	Perturbation velocity in x-direction due to singularities
v	Perturbation velocity in y-direction due to singularities
V_L	Blade surface local velocity
V_m	Cascade vector mean velocity
V_{m_x}	Component of V_m in x-direction
V_{m_y}	Component of V_m in y-direction
V_t	Tangential component of velocity
$2 \Delta V_t$	Difference between inlet and outlet tangential velocities
V_1	Cascade inlet velocity
V_2	Cascade outlet velocity
W	Velocity potential
x, y	Coordinates of rectangular axes
$\overline{x}, \overline{\phi}$	Terms associated with integration
y_ℓ	Combined blade profile lower ordinate
y_s	Slope line ordinate
y_t	Thickness ordinate
y_u	Combined profile upper ordinate
z	Complexcoordinate ($=x + iy = re^{i\theta}$)
α_1	Inlet flux angle
α_2	Outlet flux angle
α_m	Vector mean flow angle
γ	Vortex strength
$\gamma(x)$	Vortex strength distribution along x-axis
ϵ	Angle between vector mean velocity and x-axis
θ	Cascade blade camber angle
λ	Cascade blade stagger angle (+ ve for compressor cascades)

ψ Stream function

Subscripts

$'$ Gradient

si Single aerofoil

R Cascade minus single aerofoil(remainder cascade)

Appendix B THE METHOD OF CONFORMAL TRANSFORMATION

B.1. The Basic Airfoil

The airfoils are spaced along the cascade at a distance π apart; this is so that when the first transformation ζ = tanh z is applied, the cascade collapses into a single contour. The basic cambered airfoil co-ordinates are therefore calculated to a chord length $\frac{\pi}{(s/c)}$ to maintain the correct space:chord ratio. For greatest accuracy the calculation is preferably performed for every point at which the airfoil is defined, (these points are hereafter referred to as the "airfoil points")

An origin is taken on the camber line at approximately 50% chord; and cartesian axes (X,Y) chosen so that the axis of X is parallel to the chord, positive direction towards the trailing edge. The co-ordinates (X,Y) of the airfoil points are calculated.

B.2 The First Transformation (ζ = tanh z)

The origin of the z-plane is chosen to coincide with that of the (X,Y) plane, the orientation of the axes (x,y) being such that the x-axis makes an angle with the X-axis equal to the stagger, in the accepted sense. The new co-ordinates of the airfoil points in the z-plane are found.

At this stage, and again later, it is seen that many points lie close to one or the other axes; and therefore the percentage error in determining x, or y as the case may be, for these points will tend to be large compared with points lying well away from both axes. To overcome this disadvantage it is strongly recommended that, having chosen the origin of the new axes, and their orientation with respect to the old axes, simple formulae be used to give the new co-ordinates. For example

$$x = (\xi - \xi')\cos K + (\eta - \eta')\sin K$$

$$y = (\eta - \eta')\cos K - (\xi - \xi')\sin K$$

In this way any percentage error should be reasonably constant over the whole airfoil. The above expressions for x and y are to be preferred to the alternative method of drawing to a large scale and measuring.

The transformation $\zeta = \tanh z$ is applied to the airfoil and infinity points, and the co-ordinates (ξ, η), together with the velocity coefficient $\left|\frac{d\zeta}{dz}\right|_o$, evaluated. The transformation has singularities given by

$$\frac{d\zeta}{dz} = 1 - \zeta^2 = 0 \text{ or } \infty$$

but Howell (B.1) has shown that these points lie outside the airfoil, and in fact the transformation is conformal for all the airfoil points.

The infinity points $(-\infty, 0)$, $(+\infty, 0)$ in the z-plane have transformed into $(-1, 0)$, $(+1, 0)$ in the ζ -plane; while the cascade has transformed into an isolated S- shaped contour, the severity of the curvature at the ends being largely dependent on the stagger.

B3. The Joukowski Transformations ($\zeta + \frac{C^2}{\zeta} = z$)

(i) The first Joukowski transformation

The origin (ξ', η') of the new z-plane is chosen at the mid-point of the line joining the leading and trailing edge points, the x-axis lying along that line and being positive towards the trailing edge. The new co-ordinates (x,y) of the airfoil and infinity points in the z-plane are calculated. The parameter C is chosen to be one quarter of the distance between leading and trailing edge points.

The Joukowski transformation is applied to every point in turn. For each z, two values of ζ are possible. Considering the Joukowski equation, it can be seen* that for the transformed contour to be described in the same sense as the original airfoil, with $|z| < 2C$, points on the upper or suction surface should take the positive root, points on the lower or pressure surface the negative root. For the infinity points, take the root having the same sign as y; if y is zero, then follow the sign of x. The velocity coefficient is also evaluated

$$\left|\frac{d\zeta}{dz}\right|_0 = \left|\frac{\zeta^2}{\zeta^2 - C^2}\right|$$

The result of the first Joukowski transformation is an irregular kidney shape.

(ii) Subsequent Joukowski Transformations

The longest straight line PQ contained by the previous contour is located, and also points P′, Q′ on it which are as near as possible to the centres of curvature of the ends of the contour P, Q respectively. If P″, Q″ are the mid-points of PP′ and QQ respectively then the origin of the new z-plane is taken at the mid-point of P″ Q″ , the x-axis lying along PQ and being positive in the general direction of the trailing edge. 4C is taken equal to P″ Q″. The new co-ordinates (x,y) of the airfoil and infinity points are calculated.

The Joukowski transformation is again applied to every point in turn, taking the root of the same sign as y; if y is zero, then following the sign of x* (here and after, $|z| > 2$ C). The velocity coefficients are again evaluated, and the resulting contour is an irregular circle.

To obtain optimum accuracy from the last (Theodorsen) transformation, the irregular circle to which it is applied should have as few irregularities as possible; hence the optimum irregular circle is sought. It can be seen that the effect of a Joukowski transformation in general is a contraction along the x-axis, and an expansion along the y-axis. This effect is controlled by the choice of axes, and the value of C. Clearly, the x-axis has been chosen to lie along PQ , as defined above, with the object of using this fact to the best advantage; also C emphasises this effect, an increase in C giving an increased contraction in the x-direction, etc. Thus by diligently orientating the axes and choosing C, the optimum irregular can be obtained from the minimum number of Joukowski transformations.

For cascades of low stagger, the optimum Joukowski transformation is usually the second; for higher staggers (giving greater curvatures on the S-shaped contour) the optimum one may be the third or even fourth.

If more than two Joukowski transformations are found to be necessary the third and subsequent ones can conveniently be taken with the same origin as the second; all that is usually necessary is a rotation of the axes and a suitable choice of C. It is usually fairly obvious when the optimum Joukowski transformation has been reached, since the next one renders the irregularities worse.

Note *

Briefly, put $z = r_{z}e^{i\beta_{z}}$, $\zeta = r_{\zeta}e^{i\beta_{\zeta}}$

then as $z \to \infty$, $\zeta \to \infty$ or 0.

but we must have $\frac{d\beta_{\zeta}}{d\beta_{z}} \geqslant 0$

$\therefore$ as $z \to \infty$, $\zeta \to \infty$.

This is the deciding factor when determining which of the quadratic roots to take.

B.4. The Last (Theodorsen) Transformation

$$\left(\sum_{1}^{n} \left[(A_r + iB_r)\, \zeta^{-r}\right] = \ell n \left[{}^{z}/\zeta\right] \right)$$

The usefulness of this transformation depends on the rapidity with which the Fourier coefficients A_r, B_r, tend to zero, (see for example, the formulae for $\left|\frac{d\zeta}{dz}\right|_0$). If the optimum irregular circle has any pronounced localised irregularities, high order coefficients are required to accommodate them. The leading edge point in the plane of the optimum irregular circle can sometimes course such a localised irregularity, and the Theodorsen transformation fails in its object. To overcome this difficulty, such a point is ignored for the purpose of the last transformation, thus enabling a rapidly converging series to be obtained. Accordingly subsequent reference to "airfoil points" should now be understood to refer to the original airfoil points, less the leading edge point. Neglecting the leading edge on the optimum irregular circle has the effect of changing slightly the nose shape of the airfoil for which the flow is determined. The "modified" shape can easily be obtained by applying the transformations in reverse to the optimum irregular circle; it will in general not differ greatly from the original profile specified.

A point in the plane of the optimum irregular circle can be conveniently expressed as

$$z = ae^{\lambda+i\phi} = ae^{\lambda}(\cos\phi + i\sin\phi)$$

while the transformed position would be

$$\zeta = ae^{\psi+i\theta} = ae^{\psi}(\cos\theta + i\sin\theta).$$

A new set of axes (x,y) is chosen in the plane of the optimum irregular circle, with the same origin as the optimum irregular circle, but with the x-axis passing in a positive direction through the $+\infty$ point. The base circle is a circle with centre at the origin, and area equal to that of the optimum irregular circle. The radius vector ae^{λ} and argument ϕ with respect to the x-axis can then be calculated for airfoil and infinity points. By linear interpolation of the graph of radius vector against argument for airfoil points, equally spaced ordinates are obtained, enabling Simpson's Rule to be used in finding the area and hence radius of the base circle.

For airfoil points, ψ will be constant, and its proximity to zero is an indication of the closeness of the base and exact circles. The function λ is evaluated for the airfoil and infinity points, and used to find ψ_0 , where

$$\psi_0 = \frac{1}{2\pi}\int_0^{2\pi} \lambda_0 \, d\theta_0$$

A_r^1 and B_r^1 are calculated from the formulae

$$A_r{}' = A_r \quad = \frac{1}{\ } \int^{2\pi} \lambda_0 \cos(r\theta_0) d\theta_0$$

$$B_r{}' = \frac{B_r}{(ae^{\psi_o})^r} = \frac{1}{\pi}\int_0^{2\pi} \lambda_o \sin(r\theta_o)d\theta_o.$$

for r = 1, 2, 3, 4, ----q. If the integrals are evaluated using equally spaced ordinates (ie. at equal intervals of θ_o), it is seen that many of the trigomometric functions occuring are recurrent, and this can greatly reduce the amount of repetitive arithmetic involved. For greatest accuracy in making a true representation of the irregular circle, ($2\pi/d\theta_o$) should be of the order fifty or sixty. The values of $A_r{}^1$ and $B_r{}^1$ are plotted, and a value of r (say p) ascertained for which subsequent values of $A_r{}^1$ and $B_r{}^1$ can be neglected. In the analysis that follows, use only the first p values of $A_r{}^1$ and $B_r{}^1$.

The transformed positions of the two infinity points is found by using Newton's method of successive approximations to solve the following equation for ψ , given λ and ϕ

$$\Delta = \lambda - \psi = \sum_1^p \left\{[A_r{}' \cos(r\theta) + B_r{}' \sin(r\theta)]e^{-r\psi}\right\}$$

These results are used to solve for θ of the infinity points, where

$$\epsilon = \phi - \theta = \sum_1^p \left\{[B_r{}' \cos(r\theta) - A_r{}' \sin(r\theta)]e^{-r\psi}\right\}$$

The transformed positions of the airfoil points are found from the following formulae

$$\epsilon_o = \phi_o - \theta_o = \sum_1^p [B_r{}' \cos(r\theta_o - A_r{}' \sin(r\theta_o)]$$

$$\left|\frac{d\zeta}{dz}\right|_o = 1 + \sum_1^p \left\{(r - 1)[A_r{}' \cos(r\theta_o) + B_r{}' \sin(r\theta_o]\right\}$$

Note:

It would seem that ψ_0 , A_r^1, B_r^1, Δ_∞, ϵ_∞, ϵ_a and $\left|\frac{d\zeta}{dz}\right|_0$ cannot be evaluated, since ϕ and not θ is known. Experience however shows that ϵ is usually very small, and so ϕ may be used for θ without great error.

The transformed positions of the infinity point could be determined by combining Δ_∞ and ϵ_∞ into one complex equation, and solving it using the method of characteristics. Also the transformed position of an airfoil point could be found by using Newton's method of successive approximations, to solve θ_0 , given ϕ_0 (e.f. the expression for ϵ_0). However, it is suggested that these two refinements are not consistent, and therefore not justified, for the following reason. The Fourier coefficients have been found using ϕ_0 for θ_0 , hence the last transformation is only mathematically consistent if this substitution is adopted throughout. When analysis on the exact circle is pursued however, θ_0 should be used, and is given by $\theta_0 = (\phi_0 - \epsilon_0)$ to a first approximation.

B.5. Velocity on the Exact Circle

Howell (B1) has shown that the velocity at a point on the exact circle is given by

$$\frac{V_0}{V_a} = f_0 + g_0 \tan(\alpha_1) + h_0 \tan(\alpha_2)$$

where
$$f_0 = \frac{1}{2r_0}\left[\frac{\sin(\theta_1)}{\frac{1}{2}(m_1+\frac{1}{m_1})+\cos(\theta_1)} + \frac{\sin(\theta_2)}{\frac{1}{2}(m_2+\frac{1}{m_2})-\cos(\theta_2)}\right]$$

$$g_0 = \frac{1}{4r_0}\left[\frac{(m_1 - \frac{1}{m_1})}{\frac{1}{2}(m_1+\frac{1}{m_1})+\cos(\theta_1)}\right]$$

$$h_0 = -\frac{1}{4r}\left[\frac{(m_2 - \frac{1}{m_2})}{\frac{1}{2}(m_2+\frac{1}{m_2})-\cos(\theta_2)}\right]$$

and $\theta_1 = \theta_0 + (\pi - \theta_{-\infty})$

$$\theta_2 = \theta_0 - \theta_{+\infty}$$

$$m_1 = e^{\psi_{-\infty}} \quad ; \quad m_2 = e^{\psi_{+\infty}}$$

$$r_0 = ae^{\psi_0}$$

α_2 is found from Joukowski's hypothesis, which demands a stagnation point at the trailing edge.

viz:

$$\tan(\alpha_2)_{T.E.} = \left[- \frac{1}{h_0} \left\{ f_0 + g_0 \tan(\alpha_1) \right\} \right]_{T.E.}$$

B.6. Velocity and Pressure Coefficient on the Airfoil in Cascade

The velocity at a point on the airfoil is obtained by multiplying the velocity at that point on the exact circle by the velocity coefficient of that point for each transformation performed. The pressure coefficient is defined as the increase in static pressure over free stream static pressure, compared with the inlet dynamic head. That is

$$C_p = \frac{p - p_1}{\frac{1}{2}\rho V_1^2} = 1 - \frac{V^2}{V_1^2}$$

but $V = V_0 \cdot \left|\frac{d\zeta}{dz}\right| \cdot \left|\frac{d\zeta}{dz}\right| \cdot \text{-----------------} \left|\frac{d\zeta}{dz}\right|$

and $V_a = V_1 \cos(\alpha_1)$.

$$\therefore C_p = 1 - \left\{ \frac{\left[f_0 + g_0 \tan(\alpha_1) + h_0 \tan(\alpha_2) \right] \left|\frac{d\zeta}{dz}\right| \cdot \left|\frac{d\zeta}{dz}\right| \cdot \text{---} \left|\frac{d\zeta}{dz}\right| \cdot}{\cos(\alpha_1)} \right\}^2$$

Appendix C METHOD OF DISTRIBUTED SINGULARITIES

C.1. Basic Theory

The theory set out in this appendix is based on an extension of classical potential flow theory, by Schlicting (C1). The fluid considered is inviscid, irrotational and incompressible. Three basic potential flows are

1. A Uniform stream

$$\nu = Ux \quad , \quad \psi = - Uy \quad , \quad V = U.$$

2. A source or sink

$$\nu = \pm \frac{q}{2\pi} \log_e r \ , \ \psi = \pm \frac{q}{2\pi} \theta \quad V_r = \pm \frac{q}{2\pi r} .$$

3. A vortex

$$\nu = \frac{\gamma}{2\pi} \theta \ , \quad \psi = - \frac{\gamma}{2\pi} \log_e r \quad V_\theta = \frac{\gamma}{2\pi r} .$$

where V_r, V_θ are the fluid velocities along and perpendicular to a radius r.

A combination of the uniform stream with singularities of varying magnitude placed at various positions can be used to produce the flow round an aerofoil. A simple extension of the analysis will then give the flow round a series of equally spaced aerofoils, that is, a cascade.

In order to solve the direct problem of deducing the pressure distribution round a given aerofoil, the singularities distributed in the potential flow plane are selected to produce a streamline matching the aerofoil prescribed. An exact way of doing this is to spread an infinite number of singularities along the blade camber line and match completely the blade form. As this is an extremely complex procedure a small, finite number of singularities is used. In previous work (C1, C2) this number has rarely exceeded three, but the authors, with the aid of Liverpool University's "Deuce" digital computer, have increased it to between fifteen and twenty. This requires the solution of thirty or more linear simultaneous equations, a task well within the scope of the computer used.

A second approximation, that the singularities are located simplify the mathematical analysis. This assumption limits calculations to blades with camber 0.1 to 0.15c (see reference C1).

Defining the vorticity distribution along the x-axis by $\gamma(x)$ and the source and sink distribution by $q(x)$;-

$$\Gamma = \int_0^c \gamma(x)\, dx \qquad (C1)$$

where Γ is the total blade vorticity, and

$$Q = \int_0^c q(x)\, dx \qquad (C2)$$

where Q is the total source distribution and is zero for a closed aerofoil.

The flow round a cambered aerofoil of finite thickness (x, y_u); (x, y_ℓ) is considered as the sum of two superimposed flows.

1) The flow over a thick blade of zero camber defined by

$$y_t = \tfrac{1}{2}(y_u - y_\ell) \qquad (C3)$$

The uncambered profile is a streamline and applying the continuity equation (see Fig.C1(a)) to an element of the blade:-

$$(V_{m_x} + u)y_t + \tfrac{1}{2}q(x)dx = \left(V_{m_x} + u + \frac{\partial u}{\partial x}\, dx\right)\left(y_t + \frac{dy_t}{dx}\, dx\right). \qquad (C4)$$

It is assumed in this equation that u does not vary with y and the component of velocity in the y-direction, v is zero. A further assumption is made that $\frac{\partial u}{\partial x}$ is small compared with u and $\frac{dy_t}{dx}$. Rearranging equation C4 the following

$$\frac{dy_t}{dx} = y_t{}' = \frac{q(x)}{2(V_{m_x} + u)}. \qquad (C5)$$

results.

2) The flow round a thin camber line or vortex sheet. The ordinates of this line are:-

$$y_s = \tfrac{1}{2}(y_u + y_\ell) \tag{C6}$$

Flow is tangential to the camber line so that at any point

$$\frac{dy_s}{dx} = y_s' = \frac{V_{m_y} + v}{V_{m_x} + u} \tag{C7}$$

see figure (C1b)

For each pair of ordinates (y_u, y_ℓ) determined from the profile a pair of equations is produced, equations C5 and C7. Thus if n pairs of ordinates are used to define the aerofoil 2n equations are produced. The equations are solved simultaneously.

C.2. Development of Equations

C.2.1. Mathematical concept

In order to solve the simultaneous equations (C5) and (C7) the following four steps are necessary:-

1) Define $q(x)$, $\gamma(x)$ in terms of a Fourier series
2) Deduce the equations for u and v the induced velocities from the singularity distribution
3) Calculate the numerical quantities associated with $q(x)$, $\gamma(x)$, u and v.
4) Substitute the above quantities into equations (C5) and (C7) with the Fourier coefficient as the unknown parameters.

C.2.2. Definition of singularities

If x is the distance along the chord from the leading edge, a new coordinate ϕ can be defined as

$$\frac{x}{c} = \tfrac{1}{2}(1 - \cos\phi). \tag{C8}$$

The source-sink and vortex distributions are written down in terms of ϕ as a series (see Glauert Ref.C3)

$$\frac{\gamma(x)}{2V_{m_x}} = A_0 \cot\frac{\phi}{2} + A_1 \sin\phi + A_2 \sin 2\phi + \dots + A_{n-1}\sin(n-1)\phi.$$

(C9)

$$\frac{q(x)}{2V_{m_x}} = B_0\left(\cot\frac{\phi}{2} - 2\sin\phi\right) + B_2 \sin 2\phi + \dots + B_n \sin n\phi$$

(C10)

where A_0, A_1 --- A_{n-1}, B_0, B_2 --- B_n are Fourier coefficients.

C.2.3. Determination of induced velocities

The velocity potential at a point z in the complex plane, induced by a singularity at another point $\bar{z}$ is

$$W = \frac{M}{2\pi}\log_e(z - \bar{z}).$$

(C11)

where M is a complex singularity, $M = Q + i\Gamma$.

The induced velocity is given by

$$u - iv = \frac{dW}{dz} = \frac{M}{2\pi}\frac{1}{z - \bar{z}}$$

(C12)

The cascade is located in the complex plane by one of the blades having its leading edge at the origin of the complex plane (z = 0) and its chord lying along the x-axis as shown in Fig.C2. The cascade tangential direction is then at an angle λ to the y-axis, where λ is the cascade stagger angle. If the spacing of the blades is s, the leading edge of each blade lies along a line

$$L = ie^{-i\lambda}$$

(C13)

with coordinates given by

$$\bar{z} = inse^{-i\lambda} \quad \text{(n an integer)}$$

(C14)

As n varies from $-\infty$ to $+\infty$, $\bar{z}$ locates each successive blade leading edge for the infinite cascade.

It has been assumed that the singularities are distributed along the chord line (see § C1), that is parallel to the x-axis. Thus any singularity on the chord of any of the cascade blades has the complex coordinate,

$$\bar{z} = inse^{-i\lambda} + \bar{x} \tag{C15}$$

where $\bar{x}$ is its distance from the blade leading edge.
The complex velocity induced at z by this singularity is, from equation (C12)

$$u - iv = \frac{M}{2\pi} \frac{1}{z - (inse^{-i\lambda} + \bar{x})} . \tag{C16}$$

The velocity induced by the sum of singularities at corresponding $\bar{x}$ positions on all the blades as n goes from $-\infty$ to $+\infty$ is then,

$$u - iv = \frac{M}{2\pi} \sum_{-\infty}^{+\infty} \frac{1}{z - (inse^{-i\lambda} + \bar{x})}$$

$$= \frac{M}{2se^{-i\lambda}} \sum_{-\infty}^{+\infty} \frac{1}{\left(\frac{\pi(z-\bar{x})}{se^{-i\lambda}} - in\pi\right)}$$

and

$$u - iv = \frac{M}{2s} e^{i\lambda} \coth\left(\frac{\pi(z-\bar{x})}{s} e^{i\lambda}\right) . \tag{C17}$$

Substituting for Γ and Q from equations (C1) and (C2) in

$$M = Q + i\Gamma$$

equation (C17) becomes

$$u - iv = \frac{e^{i\lambda}}{2} \frac{c}{s} \int_{\frac{\bar{x}}{c}=0}^{1} \left[q\left(\frac{\bar{x}}{c}\right) + i\gamma\left(\frac{\bar{x}}{c}\right)\right] \coth\left(\pi\frac{(z - \bar{x})}{s} e^{i\lambda}\right) d\left(\frac{\bar{x}}{c}\right) \tag{C18}$$

To simplify the calculation the induced velocity is derived along the x-axis only. In the limit, as $z \rightarrow x$, equation (C18) becomes

$$u-iv = \pm \frac{\gamma(x)-iq(x)}{2} + \frac{e^{i\lambda}}{2}\frac{c}{s}\int_{\frac{\bar{x}}{c}=0}^{1}\left[q\left(\frac{\bar{x}}{c}\right)+i\gamma\left(\frac{\bar{x}}{c}\right)\right]\coth\left(\pi e^{i\lambda}\frac{(x-\bar{x})}{s}\right)d\left(\frac{\bar{x}}{c}\right) \qquad (C19)$$

As $s \rightarrow \infty$ equation (C19) becomes that for a single aerofoil, and in the limit (see reference C2)

$$u_{si}-iv_{si} = \pm \frac{\gamma(x)-iq(x)}{2} + \frac{c}{2\pi}\int_{\frac{\bar{x}}{c}=0}^{1}\left[q\left(\frac{\bar{x}}{c}\right)+i\gamma\left(\frac{\bar{x}}{c}\right)\right]\frac{d\bar{x}}{x-\bar{x}}, \qquad (C20)$$

where suffix "si" refers to the single aerofoil.

Both the induced velocity for the whole cascade and that for the single aerofoil becomes infinite at $x = \bar{x}$, a singular point in the complex plane. By subtracting the single aerofoil velocity from the cascade velocity the singular point is eliminated. The resulting velocity is known as the induced velocity for the "remainder" cascade so that

$$u_R - iv_R = (u - u_{si}) - i(v - v_{si}) \qquad (C21)$$

"R" refering to the remainder cascade, and

$$u_R - iv_R = \frac{1}{2}\frac{c}{s}\int_{\frac{\bar{x}}{c}=0}^{1}\left[q\left(\frac{\bar{x}}{c}\right)+i\gamma\left(\frac{\bar{x}}{c}\right)\right]e^{i\lambda}\left[\coth\left(\pi e^{i\lambda}\frac{x-\bar{x}}{s}\right)-\frac{e^{-i\lambda}}{\pi}\cdot\frac{s}{(x-\bar{x})}\right]d\left(\frac{\bar{x}}{c}\right) \qquad (C22)$$

Substituting for $\gamma(x)$, $q(x)$ from equations (C9) and (C10) equation (C20) is integrated explicitly. Equation (C22) must be integrated numerically.

Finally $u = u_{si} + u_R$ (C23)

$v = v_{si} + v_R$ (C24)

C.2.4. Numerical parameters

The left hand side of each of equations (C5) and (C7) comprises a numerical quantity defining the aerofoil profile at a given abscissa (distance along the chord) x. If the profile is defined at n positions the quantities on the right hand side of each equation q(x), u and v must be determined explicitly for the n corresponding values of x. For n pairs of equations, n terms of each Fourier series can be found (equations (C9) and (C10)). These terms replace $q\left(\frac{x}{c}\right)$, $\gamma\left(\frac{x}{c}\right)$ in equation (C20) and (C22) which are integrated for each value of x. This requires n integrations for each equation, or term by term n^2 integrations. This number is doubled by taking the real and imaginary parts of the equation separately.

For the single aerofoil from equation (C20)

$$u_{si} = \pm \frac{\gamma(x)}{2} + \frac{c}{2\pi}\int_{\frac{\bar{x}}{c}=0}^{1} \frac{q(\bar{x})}{x - \bar{x}}\, d\bar{x} \tag{C25}$$

$$v_{si} = \pm \left(\frac{-q(x)}{2}\right) + \frac{c}{2\pi}\int_{\frac{\bar{x}}{c}=0}^{1} \frac{\gamma(\bar{x})}{(x - \bar{x})}\, d\bar{x} \tag{C26}$$

Substituting for $q(\bar{x})$ and $\gamma(\bar{x})$ from (C9) and (C10) and writing

$$\frac{\bar{x}}{c} = \tfrac{1}{2}(1 - \cos\bar{\phi}) \quad , \quad \frac{x}{c} = \tfrac{1}{2}(1 - \cos\phi)$$ equations (C25)

and (C26) are integrated to give:-

$$\frac{u_{si}}{V_{m_x}} = \pm(A_0\cot\tfrac{\phi}{2}+A_1\sin\phi+\ldots A_{n-1}\sin(n-1)\phi+\{B_0(1+2\cos\phi)-B_2\cos2\phi - \ldots - B_n\cos(n\phi)\}. \tag{C27}$$

and

$$\frac{v_{si}}{V_{m_x}} = (-A_0+A_1\cos\phi+\ldots+A_{n-1}\cos(n-1)\phi)\pm(B_0(\cot\tfrac{\phi}{2}-2\sin\phi)+B_2\sin2\phi\ldots+B_n\sin n\phi) \tag{C28}$$

Equation (C22) must be integrated numerically. Writing for $e^{i\lambda}$

$$e^{i\lambda} = \cos\lambda + i\sin\lambda \tag{C29}$$

the integrand may be split into real and imaginary parts.

Let $F = e^{i\lambda}\left\{\coth\left(\pi e^{i\lambda}\left(\frac{x-\bar{x}}{s}\right)\right) - \frac{e^{-i\lambda}}{\pi}\frac{s}{x-\bar{x}}\right\} = F(\lambda, \frac{s}{c}, \bar{x})$ (C30)

$$F = (\cos\lambda + i\sin\lambda)\coth\left[\pi(\cos\lambda + i\sin\lambda)\frac{x-\bar{x}}{s}\right] - \frac{1}{\pi}\frac{s}{x-\bar{x}}, \tag{C31}$$

from which follow the real and imaginary parts of F,

$$F = R(F) + i\,I(F) \quad \text{and} \tag{C32}$$

$$R(F) = \frac{\cos\lambda\sinh[2\pi\frac{x-\bar{x}}{s}\cos\lambda]+\sin\lambda\sin[2\pi\frac{x-\bar{x}}{s}\sin\lambda]}{\cosh[2\pi\frac{x-\bar{x}}{s}\cos\lambda]-\cos[2\pi\frac{x-\bar{x}}{s}\sin\lambda]} - \frac{s}{\pi(x-\bar{x})} \tag{C33}$$

$$I(F) = \frac{\sin\lambda\sinh[2\pi\frac{x-\bar{x}}{s}\cos\lambda]-\cos\lambda\sin[2\pi\frac{x-\bar{x}}{s}\sin\lambda]}{\cosh[2\pi\frac{x-\bar{x}}{s}\cos\lambda]-\cos[2\pi\frac{x-\bar{x}}{s}\sin\lambda]}. \tag{C34}$$

Rewriting equation (C22) gives

$$u_R - iv_R = \frac{1}{2}\frac{c}{s}\int_{\frac{\bar{x}}{c}=0}^{1}\left[\left\{q\left(\frac{\bar{x}}{c}\right)+i\gamma\left(\frac{\bar{x}}{c}\right)\right\}\left(R(F)+iI(F)\right)\right] d\left(\frac{\bar{x}}{c}\right) \tag{C35}$$

so that

$$u_R = \frac{1}{2}\frac{c}{s}\int_{\frac{\bar{x}}{c}=0}^{1}\left[R(F)q\left(\frac{\bar{x}}{c}\right)-I(F)\gamma\left(\frac{\bar{x}}{c}\right)\right]d\left(\frac{\bar{x}}{c}\right) \tag{C36}$$

and

$$v_R = -\frac{1}{2}\frac{c}{s}\int_{\frac{\bar{x}}{c}=0}^{1}\left[I(F)q\left(\frac{\bar{x}}{c}\right)+R(F)\gamma\left(\frac{\bar{x}}{c}\right)\right]d\left(\frac{\bar{x}}{c}\right). \tag{C37}$$

Putting in the quantities for $\gamma(\bar{x})$, $q(\bar{x})$ from equations (C9) and (C10) produces integral equations in terms of the Fourier coefficients, R(F), I(F) and trignometrical values of $\bar{\phi}$. (C36) and (C37) then become

$$\frac{u_R}{V_{m_x}} = \frac{c}{s}\int_{\frac{x}{c}=0}^{1}\Big[\Big\{B_0(\cot\frac{\bar\phi}{2}-2\sin\bar\phi)+B_2\sin2\bar\phi+\dots+B_n\sin n\bar\phi\Big\}R(F)-\Big\{A_0\cot\frac{\bar\phi}{2}+A_1\sin\bar\phi+\dots+A_n\sin n\bar\phi\Big\}I(F)\Big]d\left(\frac{\bar x}{c}\right). \tag{C38}$$

$$\frac{v_R}{V_{m_x}} = -\frac{c}{s}\int_{\frac{x}{c}=0}^{1}\Big[\Big\{B_0(\cot\frac{\bar\phi}{2}-2\sin\bar\phi)+B_2\sin2\bar\phi+\dots+B_n\sin n\bar\phi\Big\}I(F)+\Big\{A_0\cot\frac{\bar\phi}{2}+A_1\sin\bar\phi+\dots+A_n\sin n\bar\phi\Big\}R(F)\Big]d\left(\frac{\bar x}{c}\right) \tag{C39}$$

These equations are integrated term by term. For ease of reference the following short hand symbols are used:-

$$f_{q_0}=-\frac{c}{s}\int\left(\cot\frac{\bar\phi}{2}-2\sin\bar\phi\right)I(F)d\left(\frac{\bar x}{c}\right) \qquad g_{q_0}=\frac{c}{s}\int\left(\cot\frac{\bar\phi}{2}-2\sin\bar\phi\right)R(F)d\left(\frac{\bar x}{c}\right)$$

$$f_{q_2}=-\frac{c}{s}\int\sin2\bar\phi I(F)d\left(\frac{\bar x}{c}\right) \qquad g_{q_2}=\frac{c}{s}\int\sin2\bar\phi R(F)d\left(\frac{\bar x}{c}\right)$$

$$f_{q_n}=-\frac{c}{s}\int\sin n\bar\phi I(F)d\left(\frac{\bar x}{c}\right) \quad (C40) \qquad g_{q_n}=\frac{c}{s}\int\sin n\bar\phi R(F)d\left(\frac{\bar x}{c}\right) \quad (C41)$$

$$f_{\gamma_0}=-\frac{c}{s}\int\cot\frac{\bar\phi}{2}R(F)d\left(\frac{\bar x}{c}\right) \qquad g_{\gamma_0}=-\frac{c}{s}\int\cot\frac{\bar\phi}{2}I(F)d\left(\frac{\bar x}{c}\right)$$

$$f_{\gamma_1}=-\frac{c}{s}\int\sin\bar\phi R(F)d\left(\frac{\bar x}{c}\right) \qquad g_{\gamma_1}=-\frac{c}{s}\int\sin\bar\phi I(F)d\left(\frac{\bar x}{c}\right)$$

$$f_{\gamma_n}=-\frac{c}{s}\int\sin n\bar\phi R(F)d\left(\frac{\bar x}{c}\right) \quad (C42) \qquad g_{\gamma_n}=-\frac{c}{s}\int\sin n\bar\phi I(F)d\left(\frac{\bar x}{c}\right) \quad (C43)$$

The limits of the integration are $\frac{\bar x}{c} = 0$ and $\frac{\bar x}{c} = 1$, and

$$d\left(\frac{\bar x}{c}\right) = \tfrac{1}{2}\sin\bar\phi\, d\bar\phi \tag{C44}$$

For $n \geq 2$ $f_{q_n} = g_{\gamma_n}$ (C45) and $f_{\gamma_n} = -g_{q_n}$ (C46)
Substituting (C40) - (C43) in (C38) and (C39).

$$\frac{u_R}{V_{m_x}} = (B_0 g_{q_0}+B_2 g_{q_2}+\dots+B_n g_{q_n}) + (A_0 g_{\gamma_0}+A_1 g_{\gamma_1}+\dots+A_n g_{\gamma_n}) \tag{C47}$$

$$\frac{v_R}{V_{m_x}} = (B_0 f_{q_0}+B_2 f_{q_2}+\dots+B_n f_{q_n}) + (A_0 f_{\gamma_0}+A_1 f_{\gamma_1}+\dots+A_n f_{\gamma_n}) \tag{C48}$$

The induced velocities on the x-axis are obtained from equations

(C23), (C24), (C27), (C28), (C47) and (C48) and are given by,

$$\frac{u}{V_{m_x}} = (B_0(1+2\cos\phi)-B_2\cos 2\phi-\ldots-B_n\cos n\phi)+(B_0 g_{q_0}+B_2 g_{q_2}+\ldots+B_n g_{q_n}) + (A_0 g_{y_0}+A_1 g_{y_1}+\ldots+A_n g_{y_n}) \quad (C49)$$

$$\frac{v}{V_{m_x}} = (-A_0+A_1\cos\phi+\ldots+A_n\cos n\phi)+(B_0 f_{q_0}+B_2 f_{q_2}+\ldots+B_n f_{q_n})+(A_0 f_{y_0}+A_1 f_{y_1}+\ldots+A_n f_{y_n}) \quad (C50)$$

Note that on the x-axis components with a ± sign disappear.

Now let

$$f_{y_0}^* = f_{y_0} - 1 \qquad g_{q_0}^* = g_{q_0} + 2\cos\phi + 1$$
$$f_{y_1}^* = f_{y_1} + \cos\phi \qquad g_{q_2}^* = g_{q_2} - \cos 2\phi$$
$$f_{y_n}^* = f_{y_n} + \cos n\phi \quad (C51) \qquad g_{q_n}^* = g_{q_n} - \cos n\phi \quad (C52)$$

so that for $n \geqslant 2$ $f_{y_n}^* = -\ g_{q_n}^*$ (C53) and

$$\frac{u}{V_{m_x}} = (A_0 g_{y_0}+A_1 g_{y_1}+\ldots+A_n g_{y_n}) + (B_0 g_{q_0}^*+B_2 g_{q_2}^*+\ldots+B_n g_{q_n}^*) \quad (C54)$$

$$\frac{v}{V_{m_x}} = (A_0 f_{y_0}^*+A_1 f_{y_1}^*+\ldots+A_n f_{y_n}^*) + (B_0 f_{q_0}+B_2 f_{q_2}+\ldots+B_n f_{q_n}) \quad (C55)$$

Equations (C54) and (C55) give the values of $\frac{u}{V_{m_x}}$, $\frac{v}{V_{m_x}}$ in terms of evaluated quatities g_y, g_q^*, f_y^*, f_q and the unknown Fourier coefficients. The evaluated quantities are in terms of ϕ, $\frac{s}{c}$ (space chord ratio) and λ (stagger angle). These results can be tabulated and used as constant parameters. The variables are then:-

1) Blade shape given by y_s', y_t'
2) Fluid inlet angle.

C.2.5. Setting up of simultaneous equations

Equations (C5) and (C7) are

$$y_t' = \frac{q(x)}{2(V_{m_x} + u)} \quad (C5) \qquad y_s' = \frac{V_{m_y} + v}{V_{m_x} + u} \quad (C7)$$

Now $\frac{\gamma(x)}{2V_{m_x}}$, $\frac{q(x)}{2V_{m_x}}$ are defined in § C.2.2.

$\frac{u}{V_{m_x}}$, $\frac{v}{V_{m_x}}$ are derived in § C.2.4.

and y_t' , y_s' appear from the aerofoil profile, see §C1.

Rearranging equations (C5) and (C7)

From (C5)

$$\frac{q(x)}{2V_{m_x}} - \frac{u}{V_{m_x}} y_t' = y_t' \tag{C56}$$

From (C7)

$$\frac{V_{m_y}}{V_{m_x}} + \frac{v}{V_{m_x}} - \frac{u}{V_{m_x}} y_s' = y_s' \tag{C57}$$

Let $\frac{V_{m_y}}{V_{m_x}}$ = K and from equations (C10), (C54) and (C55)

$$B_0(\cot\frac{\phi}{2}-2\sin\phi) + B_2\sin2\phi+\ldots+B_n\sin(n\phi)-(A_0g_{\gamma_0}+A_1g_{\gamma_1}+\ldots+A_ng_{\gamma_n})\,y_t'$$
$$-(B_0g_{q_0}^*+B_2g_{q_2}^*+\ldots+B_ng_{q_n}^*)y_t' = y_t' \tag{C58}$$

$$K+(A_0f_{\gamma_0}^*+A_1f_{\gamma_1}^*+\ldots+A_nf_{\gamma_n}^*)+(B_0f_{q_0}+B_2f_{q_2}+\ldots+B_nf_{q_n})$$

$$-(A_0g_{\gamma_0}+A_1g_{\gamma_1}+\ldots+A_ng_{\gamma_n})y_s' - (B_0g_{q_0}^*+B_2g_{q_2}^*+\ldots+B_ng_{q_n}^*)y_s' = y_s' \tag{C59}$$

Using a further substitution of P, Q, R, S

$$A_0P_0 + A_1P_1 +\ldots+A_nP_n + B_0R_0 + B_2R_2 +\ldots+ B_nR_n = -K + y_s' \tag{C60}$$

$$-A_0S_0 - A_1S_1 -\ldots-A_nS_n + B_0Q_0 + B_2Q_2 +\ldots+ B_nQ_n = y_t' \tag{C61}$$

in which:-

$$P_0=f_{\gamma_0}^*-g_{\gamma_0}\ ,\ Q_0=\cot\frac{\phi}{2}-2\sin\phi-y_t'g_{q_0}^*\ ,\ R_0=f_{q_0}-g_{q_0}^*\ ,\ S_0=y_t'g_{\gamma_0}$$

$$P_n=f_{\gamma_n}^*-g_{\gamma_n}\ ,\ Q_n=\sin n\phi-y_t'g_{q_n}^*\ ,\ R_n=f_{q_n}-g_{q_n}^*\ ,\ S_n = y_t'g_{\gamma_n} \tag{C62}$$

For each point on the profile a pair of simultaneous equations as above are produced. For n points defined, there are 2n equations and the matrix has $(2n)^2$ elements on the left hand side. As the equations stand it would be necessary to produce a solution for each angle of inlet flow required, as the value of K $\left(= \frac{V_{m_y}}{V_{m_x}}\right)$ depends on the inlet angle. It is useful therefore to split the matrix into two, one independant of K and one including K, and to solve the matricies separately. The solution then applies for all values of K. Writing:-

$$A_0 = A_{00} + KA_{0\beta} \qquad B_0 = B_{00} + KB_{n\beta}$$
$$A_n = A_{n0} + KA_{n\beta} \qquad B_n = B_{n0} + KB_{n\beta} \qquad (C63)$$

substituting in equations (C60) and (C61) and separating out the K terms, the final two sets of simultaneous equations are produced,

$$A_{00}P_0 + A_{10}P_1 + \dots + A_{n0}P_n + B_{00}R_0 + B_{20}R_2 + \dots + B_{n0}R_n = y_s'$$
$$-A_{00}S_0 - A_{10}S_1 - \dots - A_{n0}S_n + B_{00}Q_0 + B_{20}Q_2 + \dots + B_{n0}Q_n = y_t' \qquad (C64)$$

$$A_{0\beta}P_0 + A_{1\beta}P_1 + \dots + A_{n\beta}P_n + B_{0\beta}R_0 + B_{2\beta}R_2 + \dots + B_{n\beta}R_n = -1$$
$$-A_{0\beta}S_0 - A_{1\beta}S_1 - \dots - A_{n\beta}S_n + B_{0\beta}Q_0 + B_{2\beta}Q_2 + \dots + B_{n\beta}Q_n = 0$$
$$(C65)$$

C.2.6. <u>The solution of the equation matrices</u>

The magnitude of each of the parameters P, Q, R, S (equation (C62)) is determined for each value of x along the chord line corresponding to the position of the measured values y_s', y_t' producing one pair of equations. The matrix is erected by calculating parameters at various values of x.

From the solution of the two matricies appears the Fourier coefficients $A_{0\beta}$ --- $A_{n\beta}$, A_{00} --- A_{n0} ; $B_{0\beta}$ --- $B_{n\beta}$, B_{00} --- B_{n0} used in subsequent calculations.

C.3. <u>Turning Angles and Pressure Distribution</u>

The circulation round an ærofoil in cascade is defined as Γ. If $2\Delta V_t$ is the change in the tangential velocity of the flow through the cascade then

$$2\Delta V_t s = \Gamma$$
$$\Delta V_t = \frac{\Gamma}{2s} \qquad (C66)$$

Substituting for Γ from equation (C1)

$$\Delta V_t = \frac{1}{2s}\int_0^c \gamma(x)\,dx \tag{C67}$$

Substituting for $\gamma(x)$ from equation (C9) and integrating,

$$\frac{\Delta V_t}{V_{m_x}} = \frac{\pi}{2}\frac{c}{s}\left(A_0 + \tfrac{1}{2}A_1\right), \tag{C68}$$

and from (C63)

$$\frac{\Delta V_t}{V_{m_x}} = \frac{\pi}{2}\frac{c}{s}\left(\left(A_{00}+\tfrac{1}{2}A_{10}\right)+K\left(A_{0\beta}+\tfrac{1}{2}A_{1\beta}\right)\right) \tag{C69}$$

From Figure 3,

$$\tan\alpha_1 = \frac{V_{m_x}\sin\lambda + V_{m_y}\cos\lambda + \Delta V_t}{V_{m_x}\cos\lambda - V_{m_y}\sin\lambda} \tag{C70}$$

Putting in the value of ΔV_t from (C69) and $K = \frac{V_{m_y}}{V_{m_x}}$

$$\tan\alpha_1 = \frac{\sin\lambda + K\cos\lambda + \frac{\pi}{2}\frac{c}{s}\left[\left(A_{00}+\tfrac{1}{2}A_{10}\right)+K\left(A_{0\beta}+\tfrac{1}{2}A_{1\beta}\right)\right]}{\cos\lambda - K\sin\lambda} \tag{C71}$$

The stagger is defined and A_{00}, A_{10}, $A_{0\beta}$, $A_{1\beta}$ are calculated from the simultaneous equations, so that if a value of α_1 is substituted in equation (C71) a value of K may be obtained.

Separating out the "K" terms,

$$K = \frac{\tan\alpha_1 - \tan\lambda - \frac{\pi}{2}\frac{c}{s}\left[A_{00}+\tfrac{1}{2}A_{10}\right]\frac{1}{\cos\lambda}}{\tan\alpha_1\tan\lambda + 1 + \frac{\pi}{2}\frac{c}{s}\left[A_{0\beta}+\tfrac{1}{2}A_{1\beta}\right]\frac{1}{\cos\lambda}} \tag{C72}$$

and the direction of outlet flow, again from Figure 3 is given by

$$\tan\alpha_2 = \frac{\tan\lambda + K - \frac{1}{\cos\lambda}\frac{\Delta V_t}{V_{m_x}}}{1 - K\tan\lambda} \tag{C73}$$

K having been calculated from equation (C72).

The velocity induced on either side of the chord line in the x-direction is,

$$V_x = V_{m_x} + u_{si} + u_R \tag{C74}$$

From equations (C27) and (C.54) the following equation is obtained,

$$\frac{V_x}{V_{m_x}} = 1 \pm \left[(A_0 \cot\frac{\phi}{2} + A_1 \sin\phi + \dots + A_n \sin n\phi) + (A_0 g_{\gamma_0} + A_1 g_{\gamma_1} + \dots + A_n g_{\gamma_n}) + (B_0 g_{q_0}^* + B_2 g_{q_2}^* + \dots + B_n g_{q_n}^*) \right] \tag{C75}$$

The positive sign in the second term refers to the suction side, the negative sign to the pressure side. The velocity on the blade surface V_L in terms of the velocity along the x-axis has been determined by Riegels (references C4 and C5) from the approximate conformal transformation of a flat plate into an ellipse of high length to thickness ratio. For an uncambered profile (reference C4)

$$\frac{V_L}{V_m} = \frac{V_x}{V_{m_x}} \frac{1}{\sqrt{1 + y_t'^2}} \tag{C76}$$

This equation is used in references C1 and C2 to obtain the pressure distribution round the profile. For a cambered profile however Riegel's recommends (reference C5) that the gradient of the cambered profile be used so that,

$$\frac{V_L}{V_{m_x}} = \frac{V_x}{V_{m_x}} \frac{1}{\sqrt{1 + y_u'^2}} \tag{C77}$$

for the upper surface, and

$$\frac{V_L}{V_{m_x}} = \frac{V_x}{V_{m_x}} \frac{1}{\sqrt{1 + y_\ell'^2}} \tag{C78}$$

for the lower surface.

Equation (C3) $\quad y_t = \frac{1}{2}(y_u - y_\ell)$ (C3)

differentiating $\quad \frac{dy_t}{dx} = y_t' = \frac{1}{2}(y_u' - y_\ell')$ (C79)

Equation (C6) $\quad y_s = \frac{1}{2}(y_u + y_\ell)$ (C6) differentiating

$$\frac{dy_s}{dx} = y_s' = \tfrac{1}{2}(y_u' + y_l') \qquad (C80)$$

Adding (C79) and (C80) $y_s' + y_t' = y_u'$) (The gradient of the upper surface)

(C81)

Subtracting (C79) from (C80) $y_s' - y_t' = y_l'$) (The gradient of the lower surface)

Substituting for y_u' , y_l' in (C77) and (C78)

$$\frac{V_L}{V_{m_x}} = \frac{V_x}{V_{m_x}} \frac{1}{\sqrt{1 + (y_s' \pm y_t')^2}} \qquad (C82)$$

where the plus sign refers to the upper surface and the minus sign to the lower surface.

The aerofoil pressure coefficient is,

$$C_p = \frac{p_L - p_1}{\frac{1}{2}\rho V_1^2} = 1 - \left(\frac{V_L}{V_1}\right)^2 \qquad (C83)$$

where

$$\frac{V_1}{V_{m_x}} = \frac{\cos\lambda - K\sin\lambda}{\sin\beta_1} \qquad (C84)$$

see Figure 3.

Equations (C66) to (C84) allow the cascade outlet angle and blade pressure distribution to be evaluated.

C.4. Calculation Checks

The following five checks may be made on the calculation:-

1) The blade lift may be found in two ways, by graphical integration of the curve of aerofoil pressure distribution, and from the fluid inlet and outlet angles. The lift coefficient is given by,

$$C_L = \frac{s}{c}\cos^2\alpha_1(\tan^2\alpha_1 - \tan^2\alpha_2)\sin\lambda + 2\cos^2\alpha_1\frac{s}{c}(\tan\alpha_1 - \tan\alpha_2)\cos\lambda \qquad (C85)$$

Both values of lift are quantities measured perpendicular to the chord as distinct from normal cascade practice of measuring lift perpendicular to the vector mean flow direction.

2) The vorticity distribution along the blade chord is given by equation (C9) and the total circulation Γ from equation (C1). Graphical integration may be performed to determine the $\gamma(x)$ circulation. The explicit integration of $\gamma(x)$ defined in equation (C67) in terms of the change in tangential velocity, is given in equation (C68).

3) The source distribution may be found from equation (C10). Graphical integration of the source distribution curve should give zero to fulfil the condition of equation (C2).

4) The recalculated aerofoil gradients may be determined using equations (C5) and (C7). $q(x)$ is found using (C10), u and v from (C49) and (C50).

5) The original aerofoil ordinates are found by integrating equations (C5) and (C7). In order to make the integration possible explicitly the equations are written in terms of a single aerofoil.

Equation (C5) is

$$\frac{dy_t}{dx} = \frac{q(x)}{2(V_{m_x} + u)} \qquad (C5)$$

Equation (C7) is

$$\frac{dy_s}{dx} = \frac{V_{m_y} + v}{V_{m_x} + u} \qquad (C7)$$

For a single aerofoil $u \ll V_{m_x}$ and is neglected so that

$$\frac{dy_t}{dx} = \frac{q(x)}{2V_{mx}} \qquad (C85)$$

$$\frac{dy_s}{dx} = K + \frac{v_{si}}{V_{mx}} \qquad (C86)$$

Substituting for $q(x)$ from equation (C10) and v_{si} from equation (C28),

$$B_0(\cot\tfrac{\phi}{2} - 2\sin\phi) + B_2\sin 2\phi + \dots + B_n\sin n\phi = \frac{dy_t}{dx} \qquad (C87)$$

$$-A_0 + A_1\cos\phi + \dots + A_{n-1}\cos(n-1)\phi = -K + \frac{dy_s}{dx} \qquad (C88)$$

$$d\left(\frac{\bar{x}}{c}\right) = \tfrac{1}{2}\sin\bar{\phi}\, d\bar{\phi}$$

(C44)

For zero angle of attack K = 0 and writing $A_0 = 0$ (see reference C1) equations (C87) and (C88) on integration become,

$$\frac{2}{c}\, y_t = B_0(\sin\phi+\tfrac{1}{2}\sin 2\phi) + \sum_{n=2}^{n} B_n\left(\frac{\sin(1-n)\phi}{2(1-n)} - \frac{\sin(1+n)\phi}{2(1+n)}\right)$$

(C89)

and

$$\frac{2}{c}\, y_s = A_1\tfrac{1}{4}(1-\cos 2\phi) + \sum_{n=2}^{n} A_n\left\{\frac{\cos(n-1)\phi}{2(n-1)} - \frac{\cos(n+1)\phi}{2(n+1)} - \frac{1}{(n-1)(n+1)}\right\}$$

(C90)

where A_n, B_n are coefficients calculated at K = 0.

C.5. Numerical values

C.5.1. Choice of integrating points

Certain quantities have to be integrated numerically e.g. f_{q_n}, g_{q_n} (equations (C40) - (C43)). The "Deuce" computer performs an integration using Simpson's rule and requires ordinates tabulated for equally spaced abscissa. As the integrations are performed with respect to $\bar{\phi}$ $\left(\frac{\bar{x}}{c} = \tfrac{1}{2}(1 - \cos\bar{\phi})\right)$ the arc of $\bar{\phi}$ from 0 to π is divided into (18) parts of 10° each giving (19) ordinates.

C.5.2. Choice of singularity points

There are three considerations which determine the position of the singularity points:-

1) The number. As a computer isused throughout the calculation the authors were not restricted to the use of three points only as other workers have been. The initial calculation was performed on a C4 base profile which is defined by 17 points. This was taken as a nominal number of singularity points and any quantity between 15 and 20 is appropriate. Fewer points would produce quicker results, more would tend to make the calculation unwieldy. It is useful to have points close together near the leading edge,

to predict the suction peak, and an approximate spacing of every 10% chord rearward of 20% chord. It was thought that with such a large number of points Schlichting's method of positioning was superfluous and was ignored.

2) The distance from the leading edge. The simultaneous equation matrix is very sensitive to large numerical values. If any one of the parameters P, Q, R, S is large, the computer equates all small parameters to zero and produces an incorrect result. Equations (C40) - (C43) show $f_{qo}, g_{qo}, f_{\gamma o}, g_{\gamma o}$ as functions of $\cot \frac{\bar{\phi}}{2}$ which is infinite at $\frac{\bar{x}}{c} = 0$. However on changing the integration function from $\frac{\bar{x}}{c}$ to $\bar{\phi}$ $\left(\frac{\bar{x}}{c} = \frac{1}{2}(1 - \cos \bar{\phi})\right)$ the $\cot \frac{\bar{\phi}}{2}$ term disappears.

$$d\left(\frac{\bar{x}}{c}\right) = \tfrac{1}{2} \sin \bar{\phi} \, d\bar{\phi}$$

$$\int \cot \frac{\bar{\phi}}{2} \, d\left(\frac{\bar{x}}{c}\right) = \int \left(\cos^2 \frac{\bar{\phi}}{2}\right) d\bar{\phi} \qquad \text{(C91)}$$

which is finite for all values of $\bar{\phi}$. Thus the integrating points may be carried up to the leading edge of the profile.

For the singularity points on the other hand, it can be seen from equation (C62) that $Q_o\left(=\cot\frac{\phi}{2} - 2\sin\phi - y_t' g_{qo}^*\right)$ become very large as $\phi \to 0$ $\left(\frac{x}{c} \to 0\right)$ To avoid having Q_o too large the first singularity is taken at 2.5% chord back from the leading edge.

3) Integration singularities. The discontinuity of integration in equation (C19) is eliminated by the use of equations (C20) and (C22). The numerical quantities may still become infinite if $x = \bar{x}$ (see for example equations (C33) and (C34)) so that the flux singularity points must be chosen so that they do not coincide with the numerical integrating points. The limit of R(F) and I(F) as $x \to \bar{x}$ is zero, but a slight discrepancy in computation will produce a large numerical quantity. If however the computer program is modified to give a result of zero when the value of R(F), I(F) rises above a certain quantity the flux singularities may be choosen at random.

C.5.3. Profile coordinates

Blade profiles are usually described using camber line and base profile ordinates. The base profile ordinates are measured perpendicular to the camber line, at a position measured along the camber line corresponding to the base profile $\frac{x}{c}$ position (see Figure C4). It has been suggested (reference C2) that the values required in the calculation y_s, y_t (equations (C3) and (C6)), may be taken as the conventional coordinates. If the profile is set out as upper and lower ordinates along the chord, on the other hand, equations (C3) and (C6) can be used directly to determine y_s, y_t. Using an interpolation program the values of y_s, y_t for every 2.5% along the chord can be determined.

C.5.4. Profile gradients

From the thickness and slope (y_t, y_s) ordinates the gradients are found using the central difference method of calculation. The Newton-Stirling formula is differentiated (reference C6), giving

$$f'_0 = \frac{1}{h}\left(\mu\delta f_0 - \frac{1}{6}\mu\delta^3 f_0 + \frac{1}{30}\mu\delta^5 f_0 - \frac{1}{140}\mu\delta^7 f_0 + \dots\right) \tag{C92}$$

where f'_0 is the 1st derivative of the function f at $x = x_0$, h is the ordinate spacing δ^n represents the n^{th} difference and μ the mean of the upper and lower n^{th} difference. The inclusion of terms up to δ^7 is satisfactory for $\frac{x}{c}$ from .125 to 0.90. Outside these values it is necessary to use the forward or backward difference formulae.

However it was found that these formulae were unreliable in these circumstances and the gradients required are taken from a scaled up drawing of the base profile and camber line by direct measurement.

As has been previously mentioned with regard to the values of P,Q,R and S, if any one of the parameters in the simultaneous equations is large compared with the rest a useless result is produced. This phenomenon also occurs with large values of the gradients, which appear near the leading and trailing edges of the profile, and comprise the right hand side of equation (C64). The error is apparent in the plotting of the pressure distribution curve as a number of "rogue" points occur (ie. a smooth pressure plot is not produced), and the integrated lift coefficient from the curve does not agree with the lift coefficient calculated from the turning angle (see C4, 1). The authors have found it necessary in these circumstances to reduce leading and trailing edge gradients, so modifying the original profile. The largest numerical gradient is that from the thickness distribution at the leading edge, which is infinite. Even at 2.5% and 5.0% the value of y_t' is sometimes too large to be accommodated and has to be reduced. Between 10% and 90% chord the plotted values of the gradients form a smooth curve. A general rule for producing a reasonable pressure distribution, ie. no "rogue" points and correct lift coefficient, would be to extrapolate the smooth gradient curve back to 0% chord, from say 10% and on to 100% chord from say 90%. At the present time this rule is arbitrary and it is necessary, if the correct result does not appear first time to adjust leading and trailing edge gradients until a consistent answer is obtained.

For a circular arc camber line the gradient is found analytically. With $\frac{x}{c}$ chordwise position and θ the camber angle

$$\frac{dy}{dx} = \frac{1 - 2\frac{x}{c}}{\sqrt{\operatorname{cosec}^2\frac{\theta}{2} - \left(2\frac{x}{c} - 1\right)^2}} \qquad \text{(C93)}$$

Appendix D ADAPTATION OF THE METHOD OF CONFORMAL TRANSFORMATION TO USE ON AN ELECTRONIC COMPUTER

D = Data R = Results

BASIC AIRFOIL

D: Basic airfoil

R: (X, Y)

CHANGE AXES

D: $\tan\psi$, ξ', η', (X, Y)

R: (x, y)

FIRST TRANSF^{N}.

D: (x, y)

R: ξ, η, $\left|\frac{d\zeta}{dz}\right|$

CHANGE AXES

D: $\tan K$, ξ', η', (ξ, η)

R: (x, y)

1st JOUK. TRANSF^{N}.

D: (x, y), C^2

R: (ξ, η), $\left|\frac{d\zeta}{dz}\right|$

CHANGE AXES

D: $\tan K$, ξ', η', (ξ, η)

R: (x, y)

SUBSEQUENT JOUK. TRANS^{N}.

D: (x, y), C^2

R: (ξ, η), $\left|\frac{d\zeta}{dz}\right|$

ARGUMENT & RADIUS VECTOR ON OPTIMUM IRREGULAR CIRCLE.

D: (ξ, η)

R: ϕ, ae^{λ}

EQUALLY SPACED ae^{λ}

D: ϕ_0, ae^{λ_0}

R: ae^{λ} (equally spaced)

OTHER PARAMETERS

D: $ae^{\lambda_{-\infty}}$, $ae^{\lambda_{+\infty}}$, ae^{λ} (equally spaced)

R: a, ψ_0, $\lambda_{-\infty}$, $\lambda_{+\infty}$, λ (equally spaced)

MODIFIED FOURIER COEFF^{N}.

D: λ (equally spaced), $\cos(r\theta_0)$, $\sin(r\theta_0)$

R: A_r', B_r'

THE INFINITY POINTS (1)

D: A_r', B_r', $\phi_{-\infty}$, $\phi_{+\infty}$, $\lambda_{-\infty}$, $\lambda_{+\infty}$

R: $\psi_{-\infty}$, $\psi_{+\infty}$.

THE INFINITY POINTS (2)

D: A_r', B_r', $\phi_{-\infty}$, $\phi_{+\infty}$, $\psi_{-\infty}$, $\psi_{+\infty}$

R: $\theta_{-\infty}$, $\theta_{+\infty}$

ROTATION OF AIRFOIL POINTS

D: A_r', B_r', ϕ_0

R: θ_0

VELOCITY COEFFICIENTS OF THEODORSEN TRANSF^{N}.

D: A_r', B_r', ϕ

R: $\left|\frac{d\zeta}{dz}\right|$

θ_1, θ_2

D: θ_0, $\theta_{-\infty}$, $\theta_{+\infty}$

R: θ_1, θ_2

f_0, g_0, h_0

D: m_1, m_2, r_0, θ_1, θ_2

R: (f_0, g_0, h_0)

AIR ANGLES

D: α_1, (f_0, g_0, h_0) T.E.

R: α_2

PRESSURE COEFFICIENT.

D: α_1, α_2, (f_0, g_0, h_0), $\left|\frac{d\zeta}{dz}\right|$, $\left|\frac{d\zeta}{dz}\right|\ldots\left|\frac{d\zeta}{dz}\right|$

R: C_p.

Appendix E ADAPTATION OF THE METHOD OF DISTRIBUTED SINGULARITIES TO USE ON AN ELECTRONIC COMPUTER

PROGRAM 1
DATA-$\frac{x}{c}$
RESULTS-ϕ

FOR PROGRAM 16

PROGRAM 2
DATA-$\bar{\phi}$
RESULTS-$\frac{\bar{x}}{c}$

FOR PROGRAM 17

PROGRAM 3
DATA-PROFILE COORDINATES(x_n, y_n)
RESULTS-ORDINATES AT INTERMEDIATE POINTS

PROGRAM 4
DATA-ORDINATES OF PROFILE
RESULTS-DIFFERENCE TABLE PARAMETERS

PROGRAM 5
DATA-DIFFERENCE TABLE PARAMETERS
RESULTS-GRADIENTS (i) y_s', (ii) y_t'

LOOP 1 y_s'

LOOP 2 y_t'

PROGRAM 6
DATA-$\frac{x}{c}$
RESULTS-GRADIENTS y_s'
(FOR CIRCULAR ARC CAMBER LINE ONLY)

NOTE 1
USE y_t' FROM PROGRAM 5
IS CAMBER LINE CIRCULAR ARC? IF SO USE RESULTS OF PROGRAM 6 IF NOT USE RESULTS OF PROGRAM 5

PROGRAM 7
DATA-$\frac{s}{c}, \lambda, \frac{x}{c}, \frac{\bar{x}}{c}$
RESULTS-R(F), I(F)

PROGRAM 8
DATA-$\frac{s}{c}, \bar{\phi}$, R(F), I(F)
$d\bar{\phi}$(SPACING OF INTEGRATING PTS.)
RESULTS $g_{\gamma_0}, g_{\gamma_1}, f_{\gamma_0}, f_{\gamma_1}, g_{q_0}, f_{q_0}$

PROGRAM 9
DATA-$\frac{s}{c}, d\bar{\phi}, \bar{\phi}$, R(F), I(F)
RESULTS-g_{q_n}, f_{q_n}

PROGRAM 10
DATA- y_s', y_t'
$g_{\gamma_0}, g_{\gamma_1}, f_{\gamma_0}, f_{\gamma_1}$,
$g_{q_0}, f_{q_0}; g_{q_n}, f_{q_n}$
RESULTS-P, Q, R, S, y_t',

PROGRAMS 11, 12, 13
DATA-P, Q, R, S, y_s' y_t'
RESULTS-$A_{n\beta} A_{n0}$;
$B_{n\beta}, B_{n0}$

PROGRAM 14
DATA-$\frac{s}{c}$, λ, α_1
$A_{0\beta}, A_{00}, A_{1\beta}, A_{10}$
RESULTS K, $\frac{\Delta V_t}{V_{m_x}}$,
α_2, C_L

PROGRAM 15
DATA- K
$A_{n\beta}, A_{n0}; B_{n\beta}, B_{n0}$
RESULTS-A_n, B_n

TO PROGRAM 16

FROM PROGRAM 15

PROGRAM 16
DATA - λ, α_1
K
A_n, B_n
y_s', y_t'
ϕ
$g_{\gamma_0}, g_{\gamma_1}, f_{\gamma_0}, f_{\gamma_1}, g_{q_0}, f_{q_0}$
g_{q_n}, f_{q_n}

FROM PROGRAM 1

FROM PROGRAM 8

FROM PROGRAM 9

RESULTS $\frac{\gamma(x)}{V_{m_x}}$, $\frac{q(x)}{V_{m_x}}$, $\frac{u}{V_{m_x}}$, $\frac{v}{V_{m_x}}$, y_t', y_s' C_{p_u}, C_{p_L}, y_s, y_t.

Appendix F REFERENCES

B1 HOWELL, A.R. Note on the theory of arbitrary aerofoils in Cascade. Philosophical Magazine, series 7 Vol.39, London 1948.

B2 CARTER, A.D.S., and HUGHES, H.P. A theoretical investigation into the effect of profile shape on the performance of aerofoils in cascade. A.R.C. R & M 2384 March, 1946

B3 THEODORSEN, T. Theory of wing sections of arbitrary shape. NACA Report No. 411. 1931.

B4 GARRICK, J.R. On the potential flow past a lattice of arbitrary aerofoils. NACA Report No.788. 1944.

B5 Rule for nominal deviation Bristol Aero-Engines Ltd., Filton, Bristol.

C1 SCHLICHTING, H. Berechnung der reibungslosen inkompressiblem Strömung für ein vorgegebenen ebenes Schaufelgitter. VDI Forschungsheft 447, 1955.

C2 SCHNEIDER, K.H. Potential flow through a cascade of known aerofoils. M.I.T. report No.32, August 1955

C3 GLAUERT, H. The elements of aerofoil and airscrew theory. Cambridge University Press, 1948.

C4 RIEGELS, F. Das Umstroemungsproblem bei inkompressiblem Potentialstroemungen. Ing-Arch. Vol.16, 1948

C5 RIEGELS, F. Aerofoil sections Butterworths, 1961.

C6 Interpolation and allied tables H.M.S.O., 1936.

C7 Deuce alphacode manual. English Electric Co.,Ltd., Kidsgrove.

C8 Deuce program number 434 (LE06/1) English Electric Co.,Ltd., Stafford.

C9 Alphacode translator, Deuce program Number 597 (ZC23T). English Electric Co.,Ltd., Kidsgrove.

C10 MILNE-THOMSON, L.M. Theoretical Hydrodynamics. MacMillan & Co.,Ltd., London, 1949.

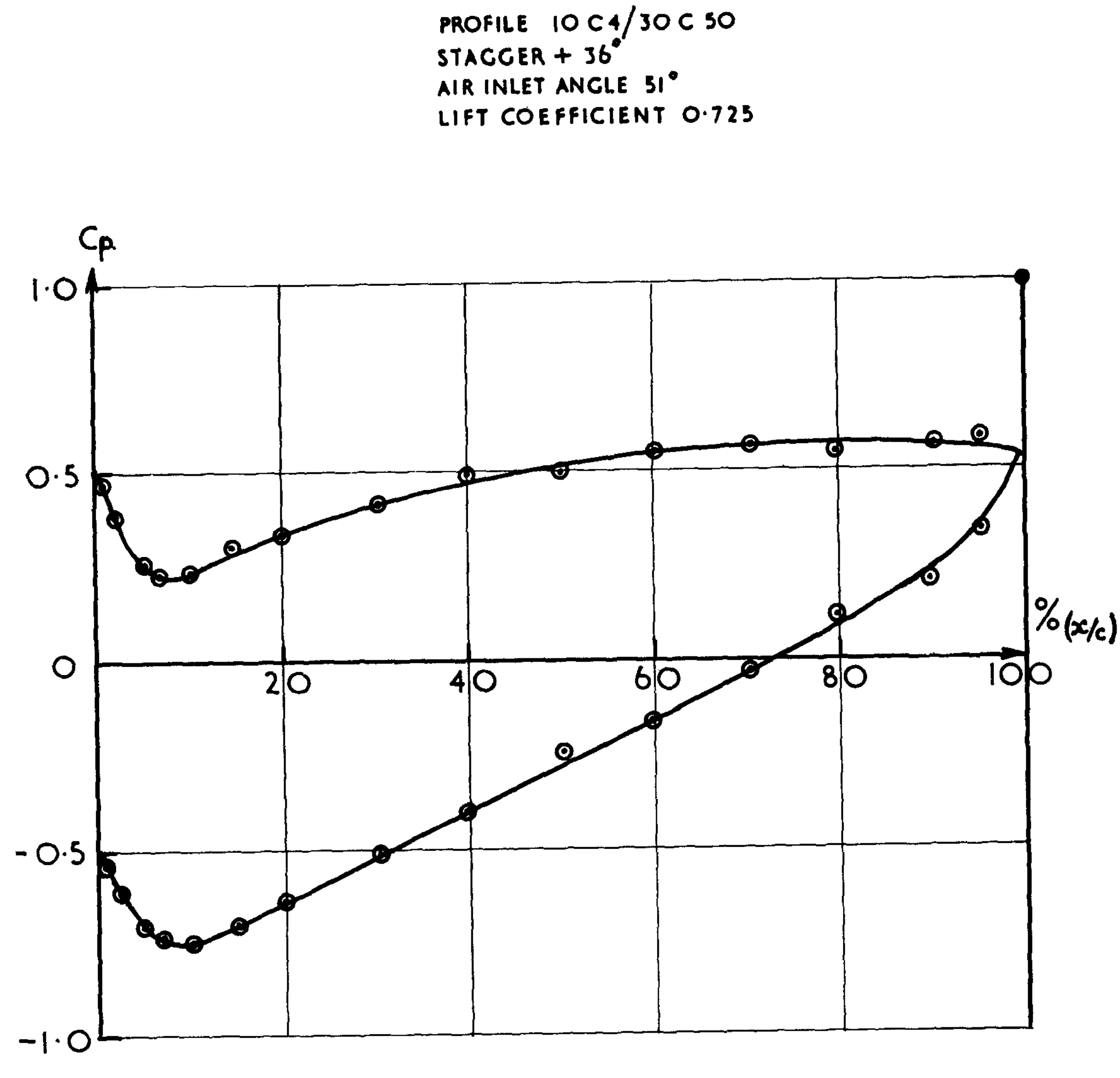

FIG. 4.1.1.
PRESSURE DISTRIBUTION.

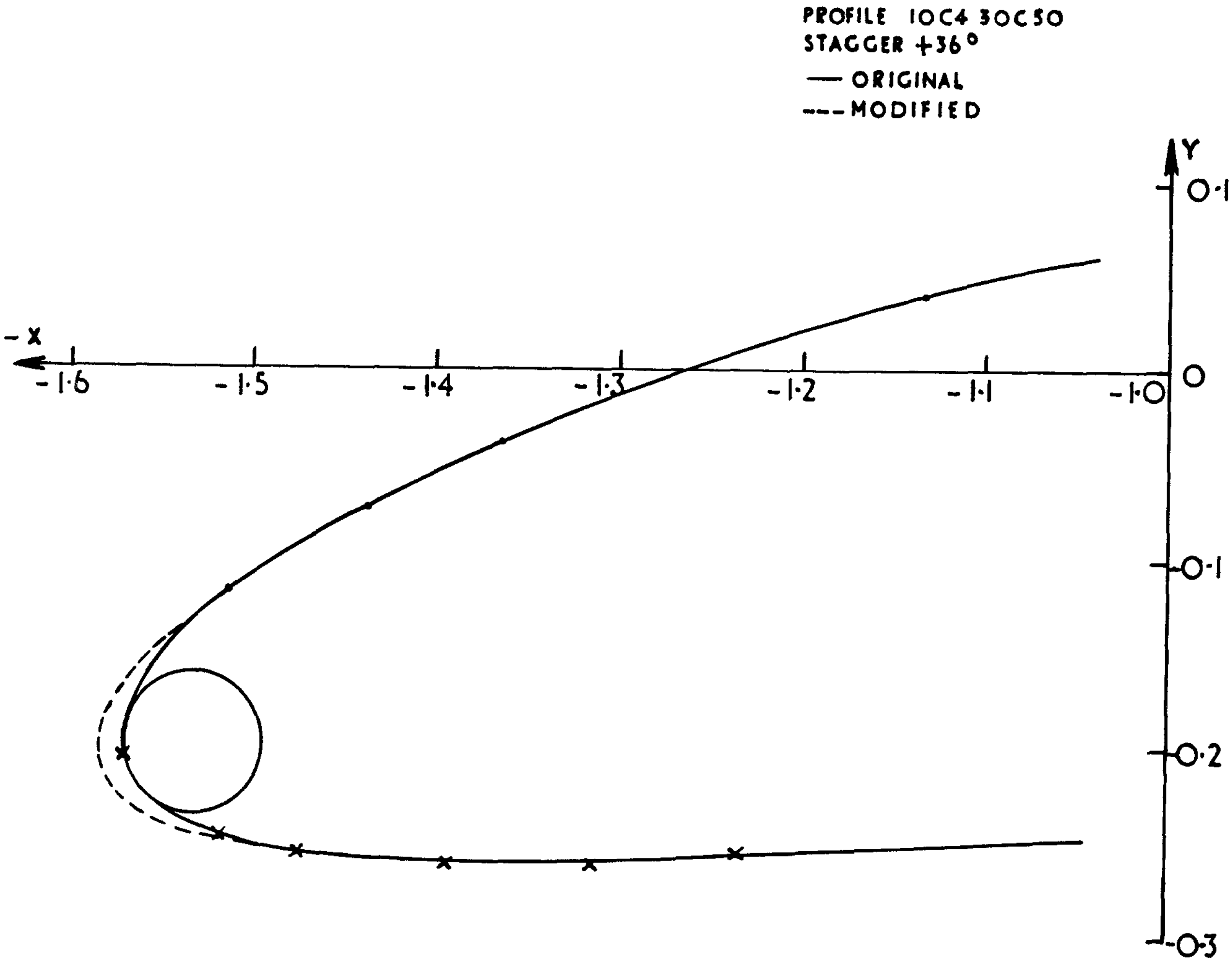

FIG. 4.1.2. ORIGINAL & MODIFIED NOSE SHAPES.

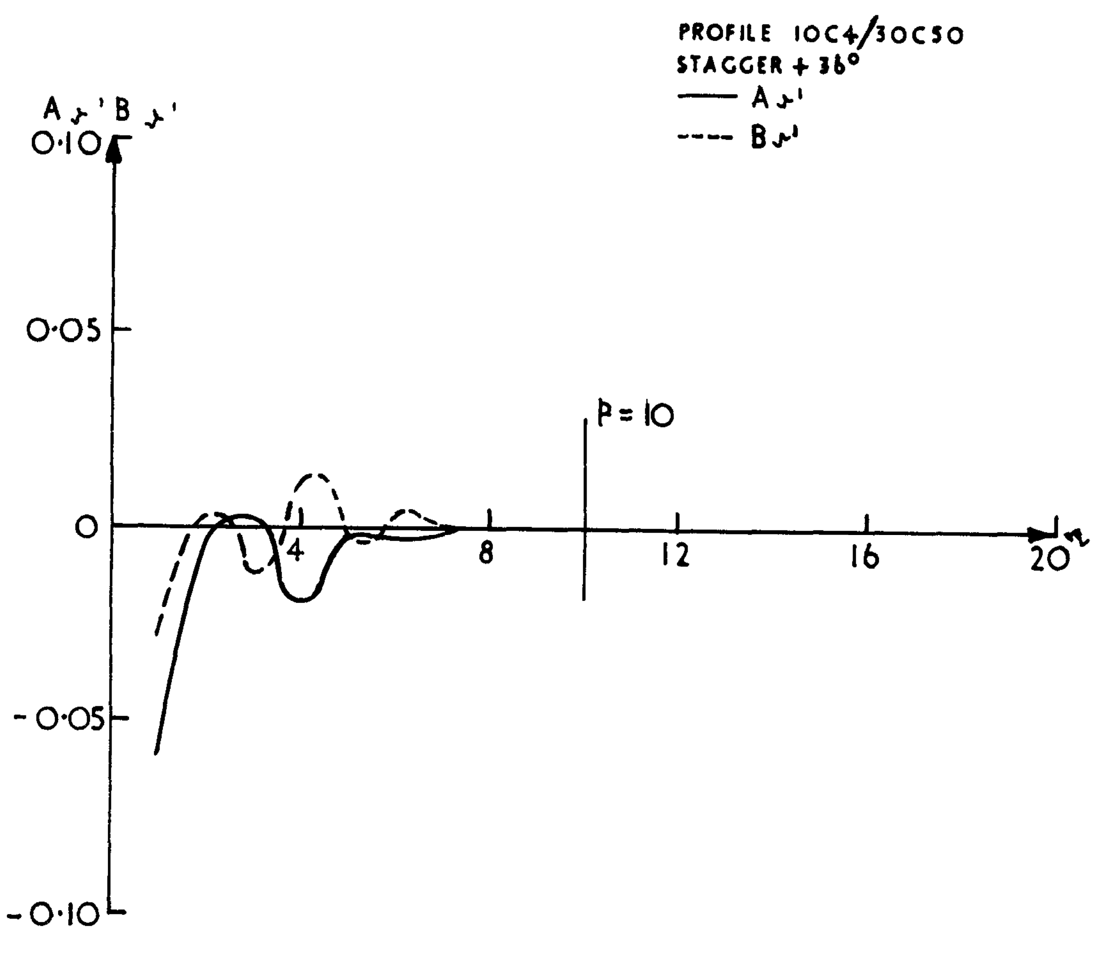

FIG. 4.1.3. MODIFIED FOURIER COEFFICIENTS.

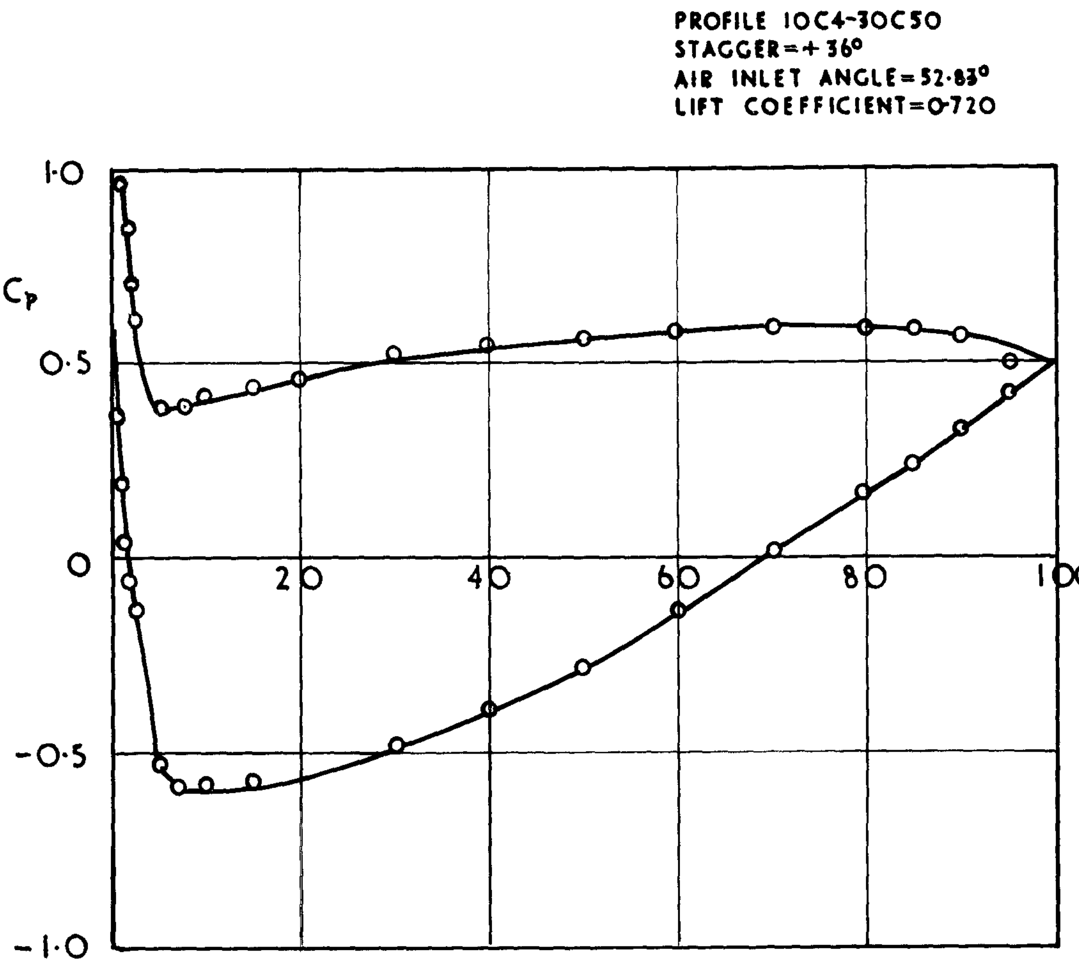

FIG. 4.2.1. PRESSURE DISTRIBUTION.

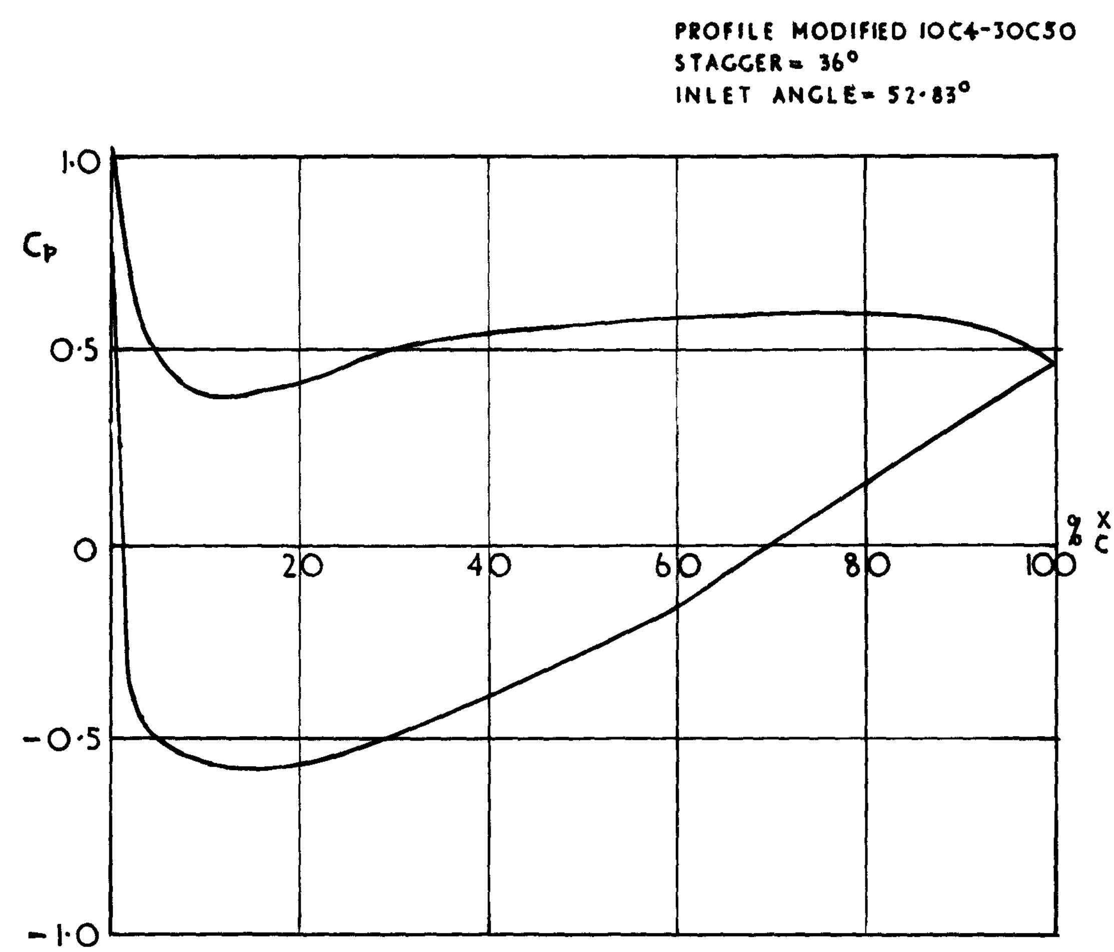

FIG. 4.2.2. PRESSURE DISTRIBUTION.

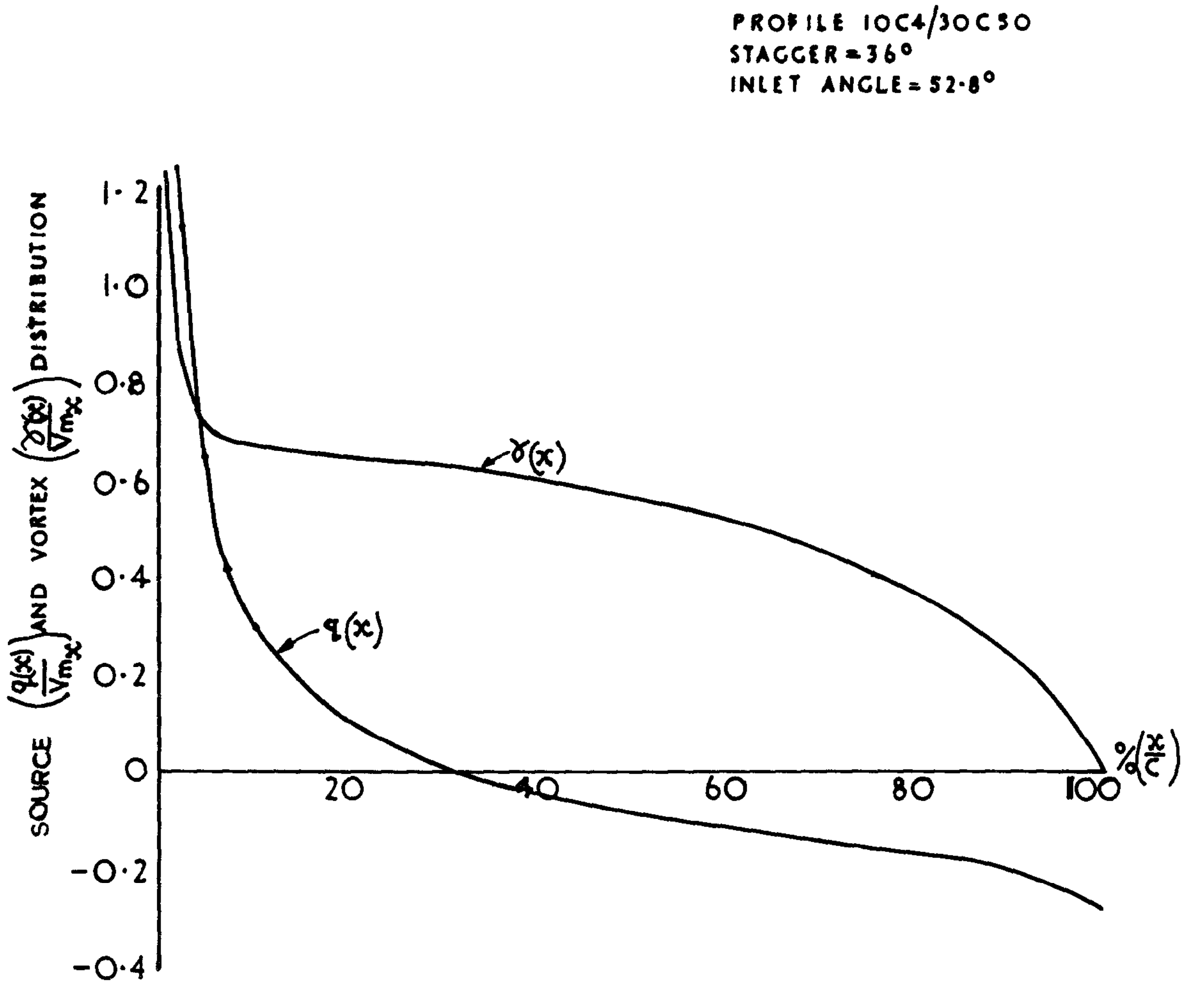

FIG. 4.2.3. DISTRIBUTION OF SOURCES AND VORTICIES.

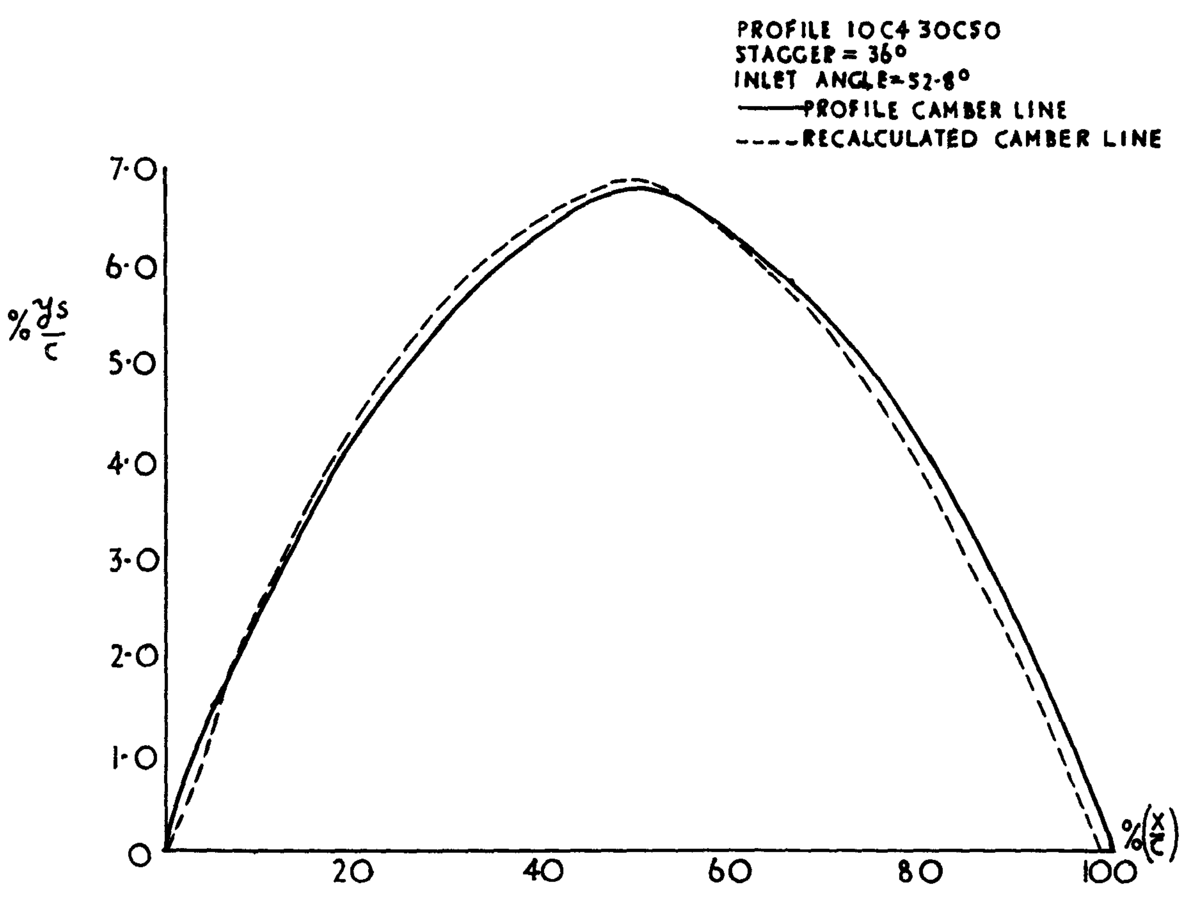

FIG. 4.2.4. COMPARISON OF PROFILE CAMBER LINE AND RECALCULATED CAMBER LINE.

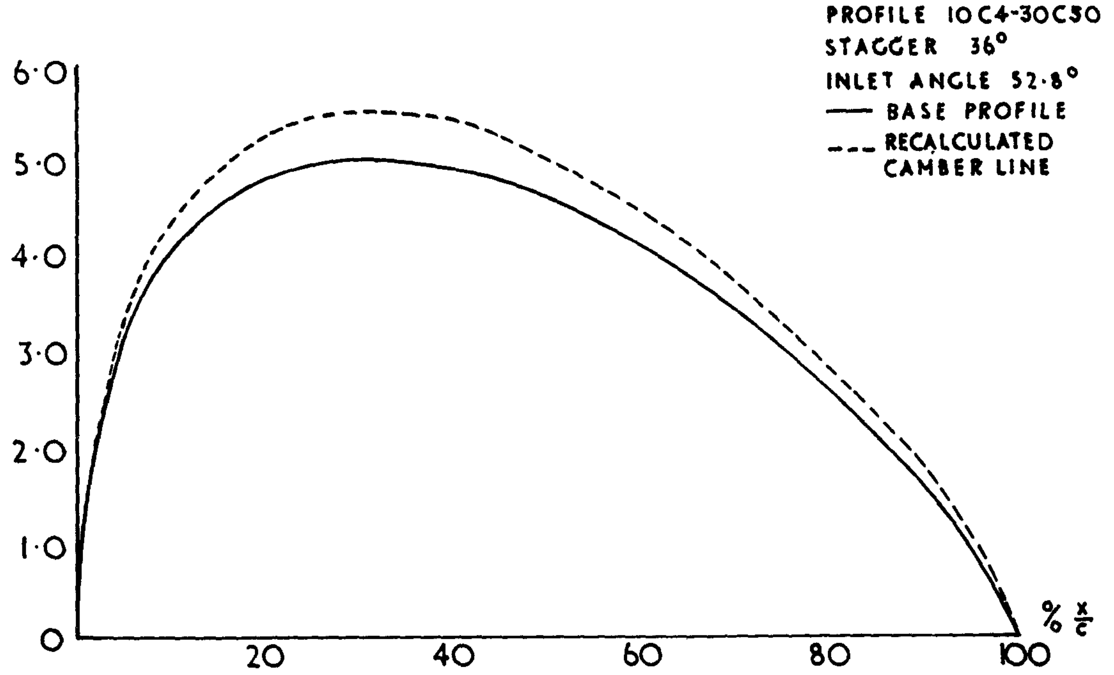

FIG. 4.2.5. COMPARISON OF BASE PROFILE AND RECALCULATED THICKNESS.

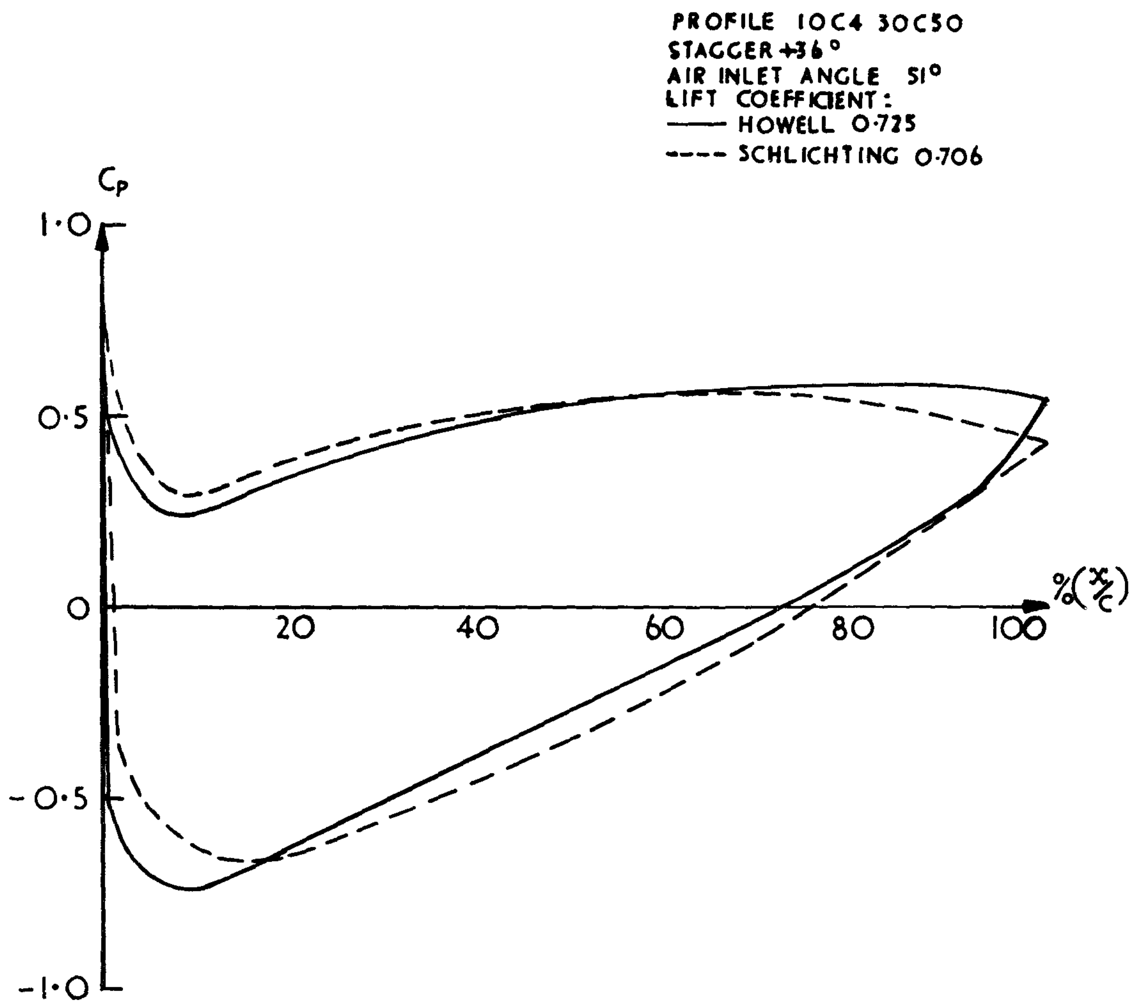

FIG.4.3.1. COMPARISON OF PRESSURE DISTRIBUTION AS DETERMINED BY THE TWO METHODS.

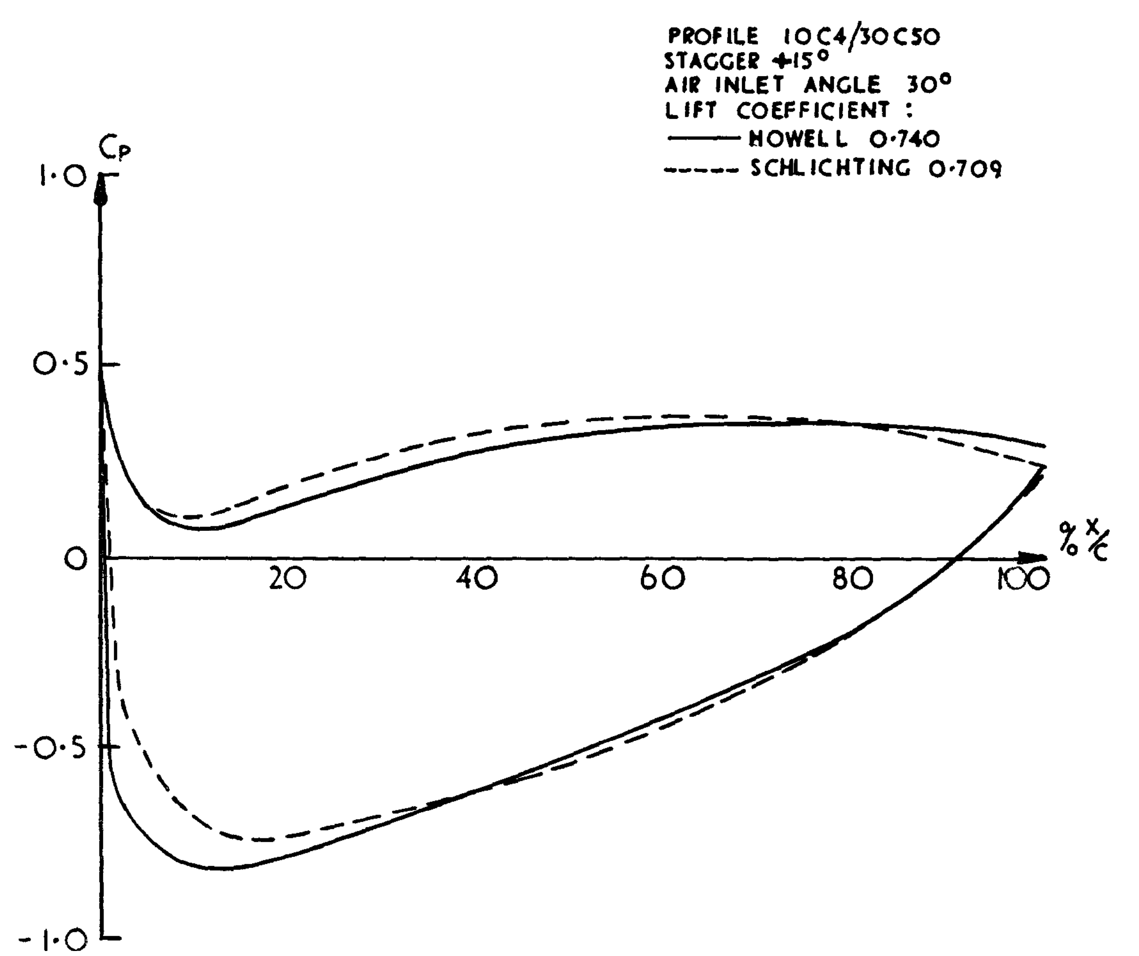

FIG.4.3.2. COMPARISON OF PRESSURE DISTRIBUTION AS

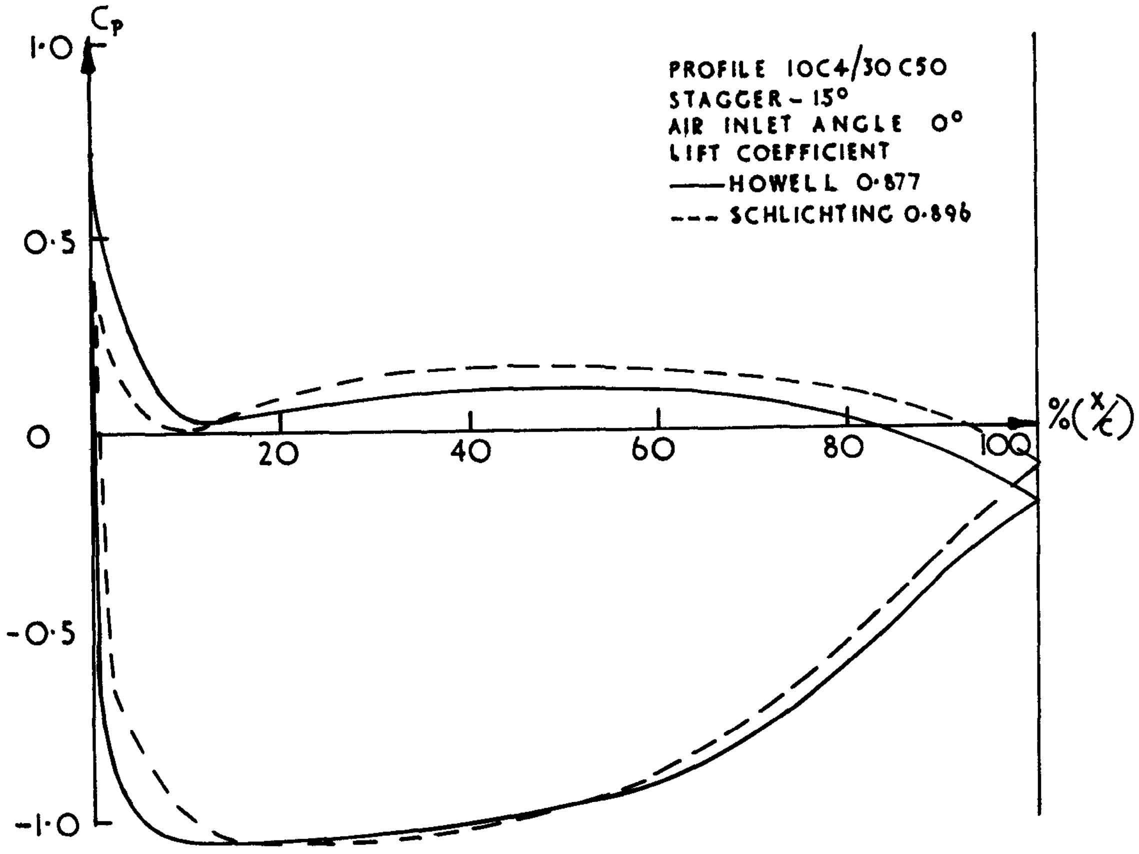

FIG.4.3.3. COMPARISON OF PRESSURE DISTRIBUTION AS DETERMINED BY THE TWO METHODS.

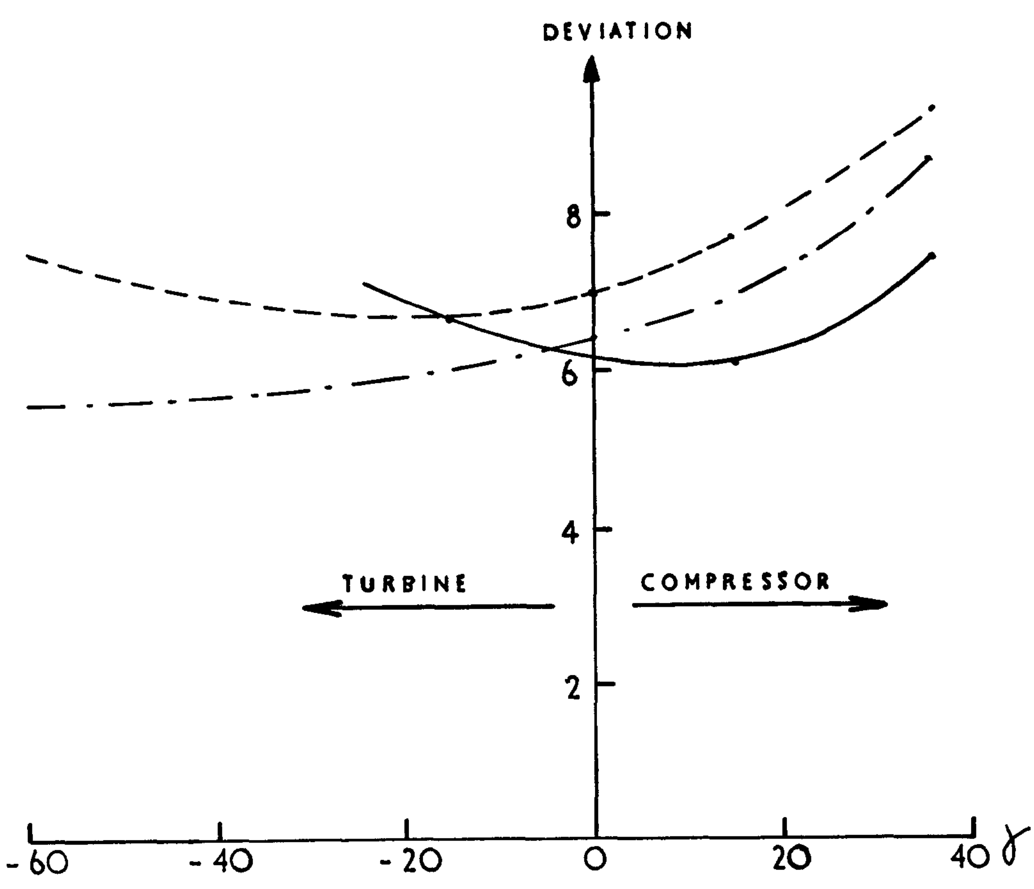

FIG. 4.3.4. DEVIATION AS A FUNCTION OF STAGGER.

——— THE METHOD OF CONFORMAL TRANSFORMATION.
- - - - - THE METHOD OF DISTRIBUTED SINGULARITIES.
—·—·—RULE FOR NOMINAL DEVIATION.

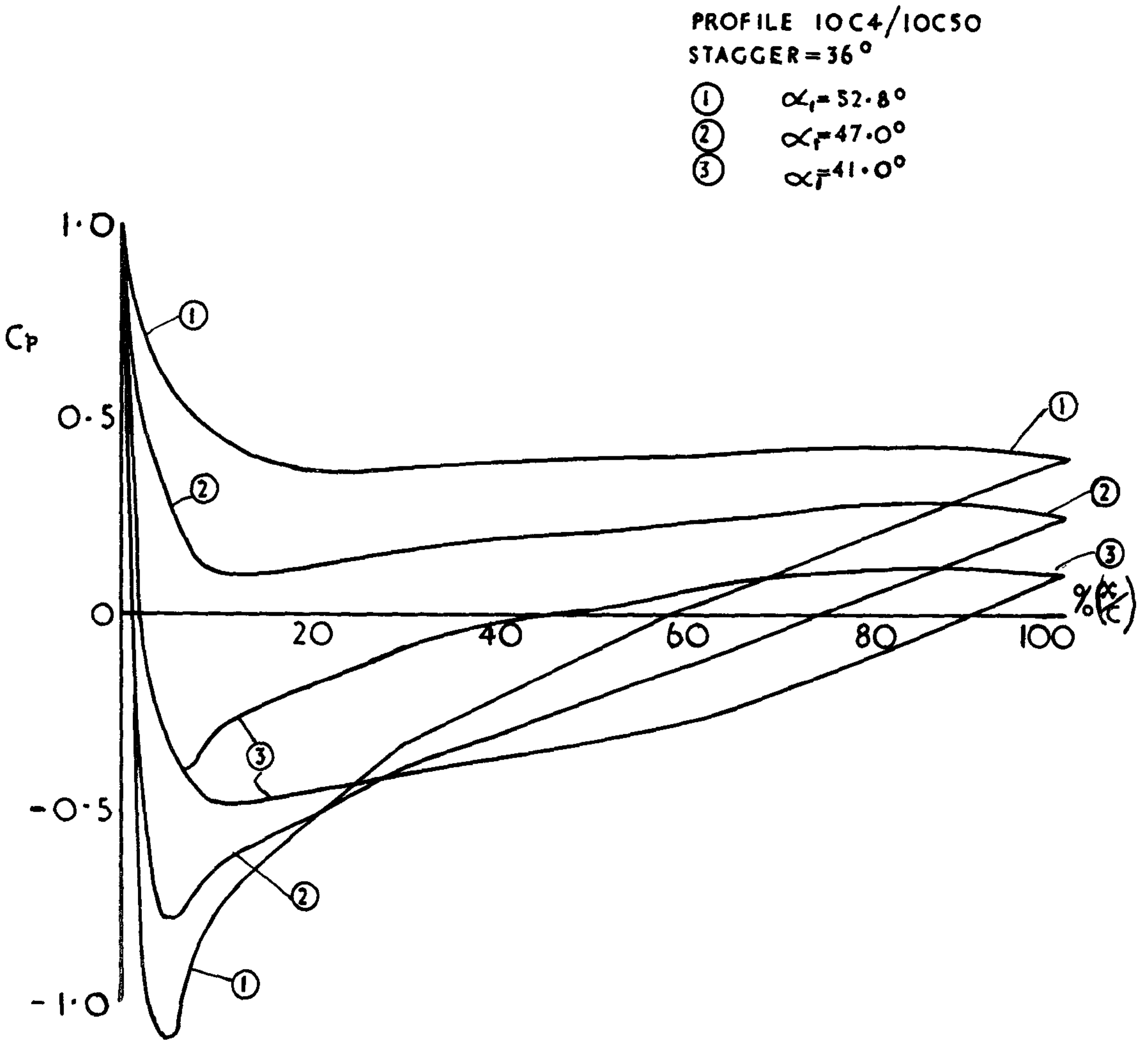

FIG. 4.4.1. PRESSURE DISTRIBUTION.

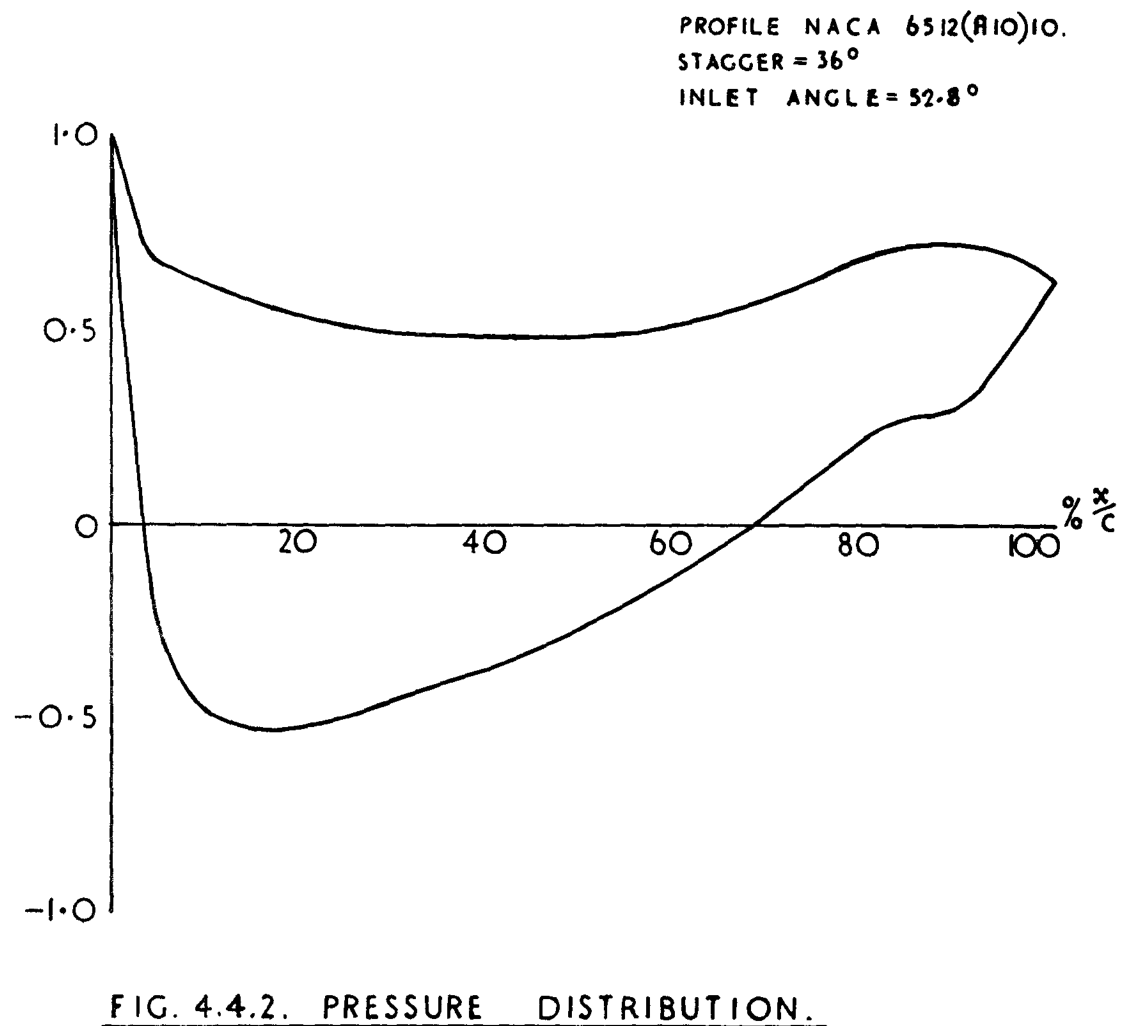

FIG. 4.4.2. PRESSURE DISTRIBUTION.

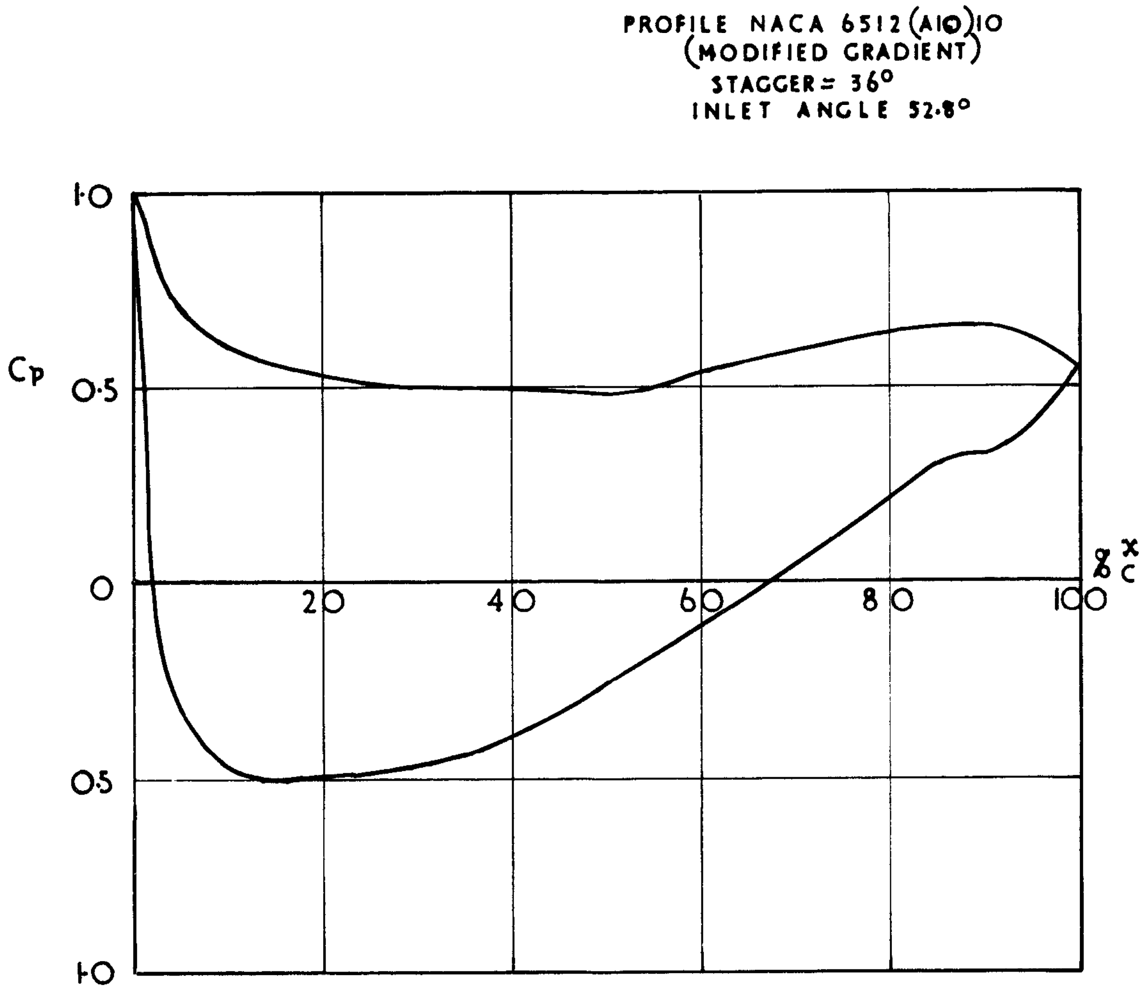

FIG. 4.4.3. PRESSURE DISTRIBUTION.

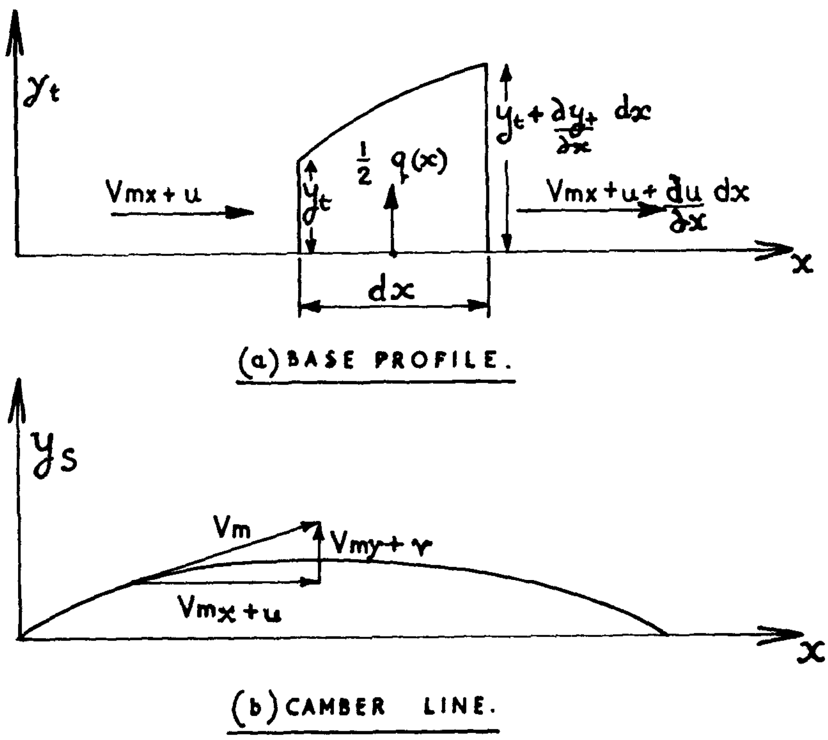

FIG. C1. FLOW CONDITIONS.

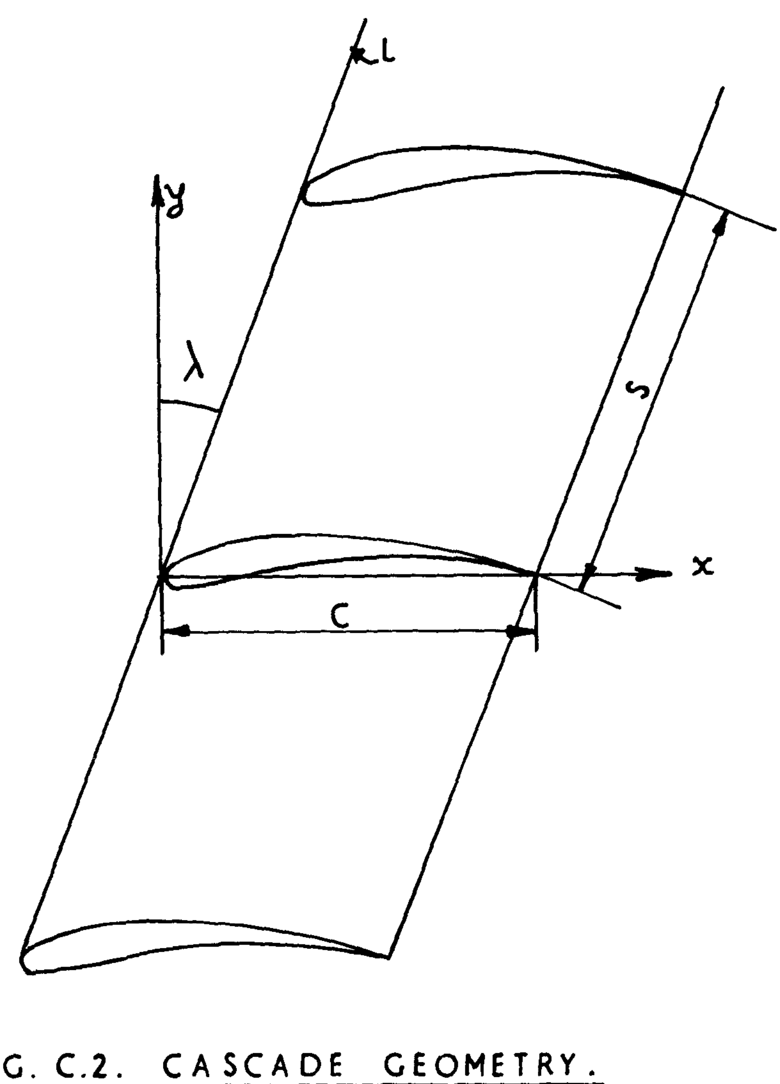

FIG. C.2. CASCADE GEOMETRY.

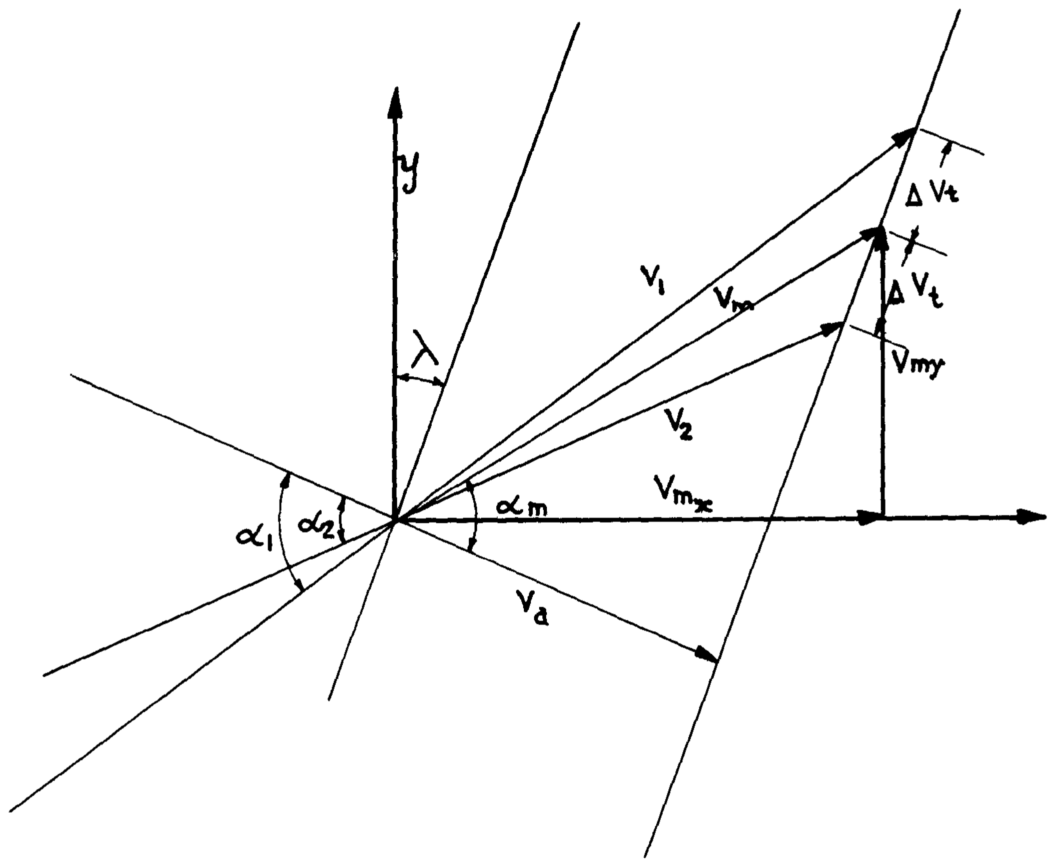

FIG. C.3.
FLUID VELOCITY TRIANGLES.

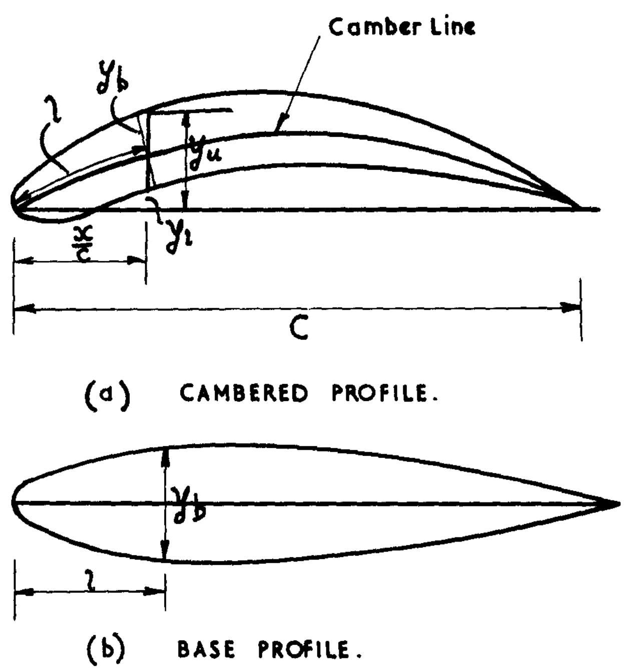

$$y_s = \frac{1}{2}(y_u + y_l)$$

$$y_t = \frac{1}{2}(y_u - y_l)$$

FIG. C.4.
BLADE PROFILE.

DS 71552/1/Wt.58 K.4 1/63 CL & XL

A.R.C. C.P. No.618
June, 1962
Pollard, D. and Wordsworth, J.

A COMPARISON OF TWO METHODS FOR PREDICTING THE POTENTIAL FLOW AROUND ARBITRARY AIRFOILS IN CASCADE

A method of conformal transformation due to Howell and a method of distributed singularities due to Schlichting, for predicting the performance of cascades of arbitrary airfoils, have been adapted for use on an electronic computer. Much greater accuracy than hitherto is thus possible, and this has enabled numerous refinements to be made. For an airfoil section defined at 30 points, the former method requires about 4 hours equally divided between automatic computing and graphical work, while the latter is completely analytical

A.R.C. C.P. No.618
June, 1962
Pollard, D. and Wordsworth, J.

A COMPARISON OF TWO METHODS FOR PREDICTING THE POTENTIAL FLOW AROUND ARBITRARY AIRFOILS IN CASCADE

A method of conformal transformation due to Howell and a method of distributed singularities due to Schlichting, for predicting the performance of cascades of arbitrary airfoils, have been adapted for use on an electronic computer. Much greater accuracy than hitherto is thus possible, and this has enabled numerous refinements to be made. For an airfoil section defined at 30 points, the former method requires about 4 hours equally divided between automatic computing and graphical work, while the latter is completely analytical

A.R.C. C.P. No.618
June, 1962
Pollard, D. and Wordsworth, J.

A COMPARISON OF TWO METHODS FOR PREDICTING THE POTENTIAL FLOW AROUND ARBITRARY AIRFOILS IN CASCADE

A method of conformal transformation due to Howell and a method of distributed singularities due to Schlichting, for predicting the performance of cascades of arbitrary airfoils, have been adapted for use on an electronic computer. Much greater accuracy than hitherto is thus possible, and this has enabled numerous refinements to be made. For an airfoil section defined at 30 points, the former method requires about 4 hours equally divided between automatic computing and graphical work, while the latter is completely analytical

and needs about 3 hours machine time (both times being for a slow code of computer operation). The two approaches are critically sensitive to profile shape. Pressure distributions as determined by each method are in close agreement, but the agreement in turning angle is only fair.

and needs about 3 hours machine time (both times being for a slow code of computer operation). The two approaches are critically sensitive to profile shape. Pressure distributions as determined by each method are in close agreement, but the agreement in turning angle is only fair.

and needs about 3 hours machine time (both times being for a slow code of computer operation). The two approaches are critically sensitive to profile shape. Pressure distributions as determined by each method are in close agreement, but the agreement in turning angle is only fair.

Printed and published by
HER MAJESTY'S STATIONERY OFFICE

To be purchased from
York House, Kingsway, London, W.C.2
423 Oxford Street, London W.1
13A Castle Street, Edinburgh 2
109 St. Mary Street, Cardiff
39 King Street, Manchester 2
50 Fairfax Street, Bristol 1
35 Smallbrook, Ringway, Birmingham 5
80 Chichester Street, Belfast 1
or through any bookseller

Printed in England

S.O. Code No. 23-9013-18

C. P. No. 618